FERMILAB-PUB-23-390-T

Prepared for submission to JCAP

Supermassive Primordial Black Holes From Inflation

Dan Hooper,[a,b,c] **Aurora Ireland,**[d] **Gordan Krnjaic,**[a,b,c] **Albert Stebbins**[c]

[a]University of Chicago, Kavli Institute for Cosmological Physics, Chicago, IL USA
[b]University of Chicago, Department of Astronomy and Astrophysics, Chicago, IL USA
[c]Fermi National Accelerator Laboratory, Theoretical Astrophysics Group, Batavia, IL USA
[d]University of Chicago, Department of Physics, Chicago, IL USA

E-mail: dhooper@fnal.gov, anireland@uchicago.edu, krnjaicg@fnal.gov, stebbins@fnal.gov

Abstract. There is controversy surrounding the origin and evolution of our universe's largest supermassive black holes (SMBHs). In this study, we consider the possibility that some of these black holes formed from the direct collapse of primordial density perturbations. Since the mass of a primordial black hole is limited by the size of the cosmological horizon at the time of collapse, these SMBHs must form rather late, and are naively in conflict with CMB spectral distortion constraints. Such limits, however, can be avoided if the distribution of primordial curvature perturbations is highly non-Gaussian. In this study, we present a model of multi-field inflation — the curvaton model supplemented with self-interactions — which can viably yield such dramatic non-Gaussinities. Furthermore, we calculate the maximal abundance of black holes that can be generated in this scenario and find this to be consistent with the observed population of high-redshift SMBHs. This result is particularly timely in light of recent evidence from the NANOGrav experiment for a stochastic gravitational wave background consistent with SMBH mergers.

Contents

1 Introduction

Supermassive black holes (SMBHs) are ubiquitous in our universe, being present in the centers of nearly all massive galaxies. Quasars,[1] powered by black holes with with masses $M \sim 10^{8-10}\, M_\odot$, are also found in large numbers in the high-redshift universe. At present, over 170 quasars have been observed at $z > 6$, with the most distant at $z = 7.54$, and several hundred others at $z = 5 - 6$ [2–10]. Fig. 1 shows the quasar abundance as a function of redshift over several ranges of black hole mass. While this magnitude limited quasar catalog is believed to be nearly complete out to $z \sim 5$, only a small fraction of SMBHs are, in fact, quasars. A more complete census of SMBHs is possible in the local universe where one finds $\Omega_{\rm SMBH}(z = 0) \sim 10^{-6}$ [11]. This contrasts with the peak quasar mass density of $\Omega_{\rm quasar}(z = 2) \sim 10^{-8}$. While specific models for SMBH population evolution have been proposed [12–14], the limited available data leaves a great deal of uncertainty.

[1] Quasars are the most luminous active galactic nuclei (AGN). In this paper, quasar refers to an AGN that is sufficiently luminous to appear in a quasar catalog such as SDSS DR7 [1]. While this definition is redshift-dependent, the most luminous quasars should be consistently present in the catalog up to the DR7 redshift limit of 5. In the text, the phrase "quasar mass" refers to the mass of the black hole that powers the quasar.

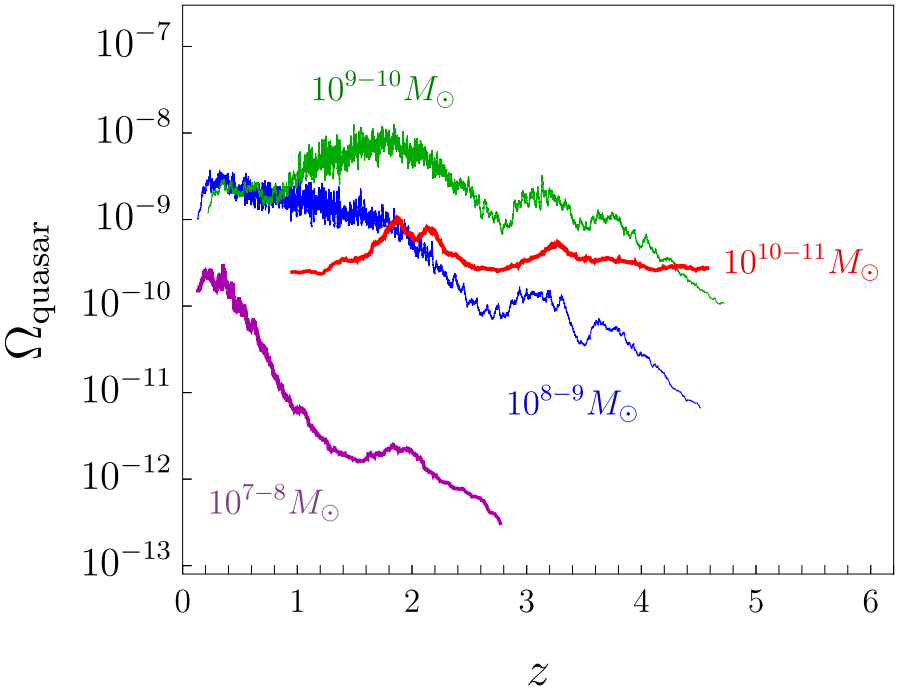

Figure 1. Estimates of the quasar black hole comoving mass density in units of the $z = 0$ critical density as a function of redshift, plotted for the four different mass classes indicated. Black hole masses and redshifts are taken from the DR7 SDSS quasar survey [1], which covers 20% of the sky and the redshift range $0 < z < 5$. The results shown represent the moving average of 100 quasars sorted by redshift.

It is usually assumed that SMBHs grow over time from relatively low-mass seeds (possibly the remnants of Population III stars [15]) through the process of accretion. The rate of mass accretion is Eddington limited to

$$\dot{M}_{\rm Edd} \lesssim \frac{M_{\rm BH}}{\tau_S}, \tag{1.1}$$

where

$$\tau_{\rm S} = \frac{\varepsilon\,\sigma_{\rm T}}{4\pi\,G\,m_{\rm p}} \approx 45\ {\rm Myr}\left(\frac{\varepsilon}{0.1}\right) \tag{1.2}$$

is the Salpeter time [16], $\sigma_{\rm T} = 8\pi\,\alpha^2/(3m_e^2)$ is the Thomson cross section, m_p is the proton mass, and ε is the radiative efficiency. At the maximum growth rate, a $10^2\,M_\odot$ black hole seed would require $\sim 0.8\,$Gyr to grow to $M \sim 10^{10}\,M_\odot$. Since $z \sim 6-7$ corresponds only to $\sim 0.7-0.9\,$Gyr after the Big Bang, such a scenario would require that the largest high-redshift black holes must have grown at high accretion rates almost continuously during the first Gyr of our universe's history. This contrasts with the intermittent accretion that SMBHs undergo at lower redshifts. From this perspective, it is surprising that so many highly-massive quasars have been observed at such high redshifts [17–21].

There is a significant population of $M_{\rm BH} \gtrsim 10^9\,M_\odot$ quasars at $z \sim 6$ to 7 [4, 22–24]. The $M_{\rm BH} \gtrsim 10^{10}\,M_\odot$ population has remained approximately constant since at least $z \sim 5$ [25] (see the red curve of Fig. 1) which, curiously, requires any growth in the number of SMBHs to be balanced by a decrease in the fraction of SMBHs that are actively quasars. Also curious

is the observation that the maximum quasar mass has not increased much since $z \sim 5$. This leaves us with two intriguing questions:

1. If these quasars grew from small black hole seeds, how did they come to be so massive on such a short timescale?

2. Why did their growth rate dramatically slow down during the subsequent 13 Gyr?

It has been suggested that the suppressed growth of the most massive black holes after the first Gyr could perhaps be attributed to galaxy-scale feedback. This, however, would require the M-σ relation[2] to evolve with redshift and for the quasar luminosity function to steepen at the highest values [26, 27]. Alternatively, it has been proposed that there might be a maximum mass that black holes can reach through accretion, resulting from the fragmentation of the accretion disks that could have otherwise facilitated rapid black hole growth [28]. Despite these suggestions, there remain many open questions concerning the origin and evolution of our universe's most massive black holes.

In this study, we take these questions to motivate another possibility: that our universe's most massive black holes did not acquire most of their mass through accretion, but are instead predominantly primordial in origin. Unlike smaller primordial black holes (PBH), these objects would have formed at later times, as governed by the size of the cosmological horizon. During the radiation dominated era, the horizon contains the following amount of energy:

$$M_H = \frac{4\pi}{3}\rho R_H^3 \approx 3 \times 10^9\, M_\odot \left(\frac{10\,\mathrm{keV}}{T}\right)^2 \left(\frac{3.36}{g_\star(T)}\right)^{1/2}, \tag{1.3}$$

where $R_H = H^{-1}$ is the size of the horizon, $\rho = \pi^2 g_\star(T) T^4/30$ is the radiation density, and $g_\star$ is the number of relativistic species at temperature T. When a sufficiently large density fluctuation collapses to form a PBH, the mass of the resulting black hole is typically an order one fraction of the horizon mass, $M_{\rm BH} \simeq \gamma\, M_H$, where $\gamma \sim 0.2$ quantifies the efficiency of collapse [29]. From Eq. (1.3), we conclude that the PBHs in the mass range of interest here form after the start of Big Bang nucleosynthesis ($T \sim$ MeV corresponds to $M_H \sim 10^5\, M_\odot$) but well before the onset of matter domination or recombination ($T \sim$ eV corresponds to $M_H \sim 3 \times 10^{17}\, M_\odot$).

Many inflationary models enable PBHs to form efficiently [30], including those in which the inflaton undergoes a period of ultra-slow-roll [31–34], or whose potential features localized bumps, dips, or steps on small scales [35–37]. More generically, a local enhancement of the power spectrum $\mathcal{P}_\zeta$ requires a deviation from slow-roll evolution (see for example, Refs. [38–51]). Regardless of the mechanism, PBH formation requires a significant enhancement in the amplitude of the primordial power spectrum. Assuming Gaussian statistics, this amplitude must be $\mathcal{P}_\zeta(k_{\rm BH}) \sim 10^{-2}$, seven orders of magnitude larger than observed on large scales, $\mathcal{P}_\zeta(k_{\rm CMB}) \simeq 2.1 \times 10^{-9}$ [52]. Such an amplification inevitably leads to large CMB spectral distortions. In particular, for scales $k_{\rm BH} \lesssim 10^5\,\mathrm{Mpc}^{-1}$, corresponding to black holes in the mass range $M_{\rm BH} \gtrsim 10^3 M_\odot$, the predicted spectral distortions are in strong conflict with COBE/FIRAS measurements [53, 54].

In principle, PBHs can form from smaller peaks in the power spectrum if the tail of the ζ distribution is sufficiently non-Gaussian. Of course, observations on large scales and

[2]The observed correlation between the velocity dispersion of a stellar bulge σ and the mass of the SMBH at its center.

measurements of the non-linearity parameters $f_{\rm NL}$ and $g_{\rm NL}$ seem to indicate that ζ is very nearly Gaussian [55, 56]. However, such perturbative measures of non-Gaussianity do not capture the tail of the distribution, where fluctuations can be large and rare [37]; it is precisely this tail that governs PBH formation.

In this paper, we quantify the degree of non-Gaussianity that would be required to viably produce primordial SMBHs and present a model of inflation that contains the necessary features. We begin in Sec. 2 by reviewing the calculation of the PBH abundance in the Press-Schechter formalism. In Sec. 3, we examine how measurements of spectral distortions constrain the primordial power spectrum, and demonstrate that the appreciable formation of SMBHs from Gaussian density fluctuations is excluded on the basis of these constraints. Sec. 4 considers departures from Gaussianity, and quantifies the heaviness of the distribution needed to evade these bounds. In Sec. 5, we review the calculation of the curvature perturbation and its statistics in the standard curvaton scenario, which has been shown to be capable of producing appreciable non-Gaussianity. This model, however, cannot viably produce a significant abundance of primoridal SMBHs, so in Sec. 6 we introduce self-interactions to augment the non-Gaussianity. We calculate the maximum PBH mass fraction that is compatible with spectral distortion bounds in this model and find that it is capable of accounting for the observed abundance of SMBHs. We conclude in Sec. 7 with a summary of our results and offer some comments on directions for future investigations.

2 Primordial Black Holes from Gaussian Perturbations

The initial abundance of PBHs is quantified in terms of their mass fraction at the time of formation:

$$\beta \equiv \frac{\rho_{\rm BH}}{\rho_{\rm tot}} \,. \tag{2.1}$$

For PBHs that formed during radiation domination, this quantity is related to the fractional energy density in black holes today, $\Omega_{\rm BH} \simeq \beta\,(1+z_f)\,\Omega_R$, where z_f is the redshift at the time of black hole formation. Using Eq. (1.3) and entropy conservation, this can be written more conveniently in terms of the initial PBH mass as:

$$\Omega_{\rm BH} \simeq 10^{-6} \left(\frac{\beta}{10^{-10}}\right) \left(\frac{\gamma}{0.2}\right)^{1/2} \left(\frac{10^8\,M_\odot}{M_{\rm BH}}\right)^{1/2} \left(\frac{g_{\star,s}(T_f)}{3.91}\right)^{1/3} \left(\frac{3.36}{g_\star(T_f)}\right)^{1/4} , \tag{2.2}$$

where T_f is the temperature at the time of black hole formation.

In the standard[3] treatment based on the Press-Schechter formalism [60], β is computed by integrating the probability distribution P_δ for the coarse-grained density contrast $\delta = \delta\rho/\bar{\rho}$ over all values greater than the critical threshold for collapse, δ_c:

$$\beta \simeq 2 \int_{\delta_c}^{\infty} d\delta\, P_\delta[\delta] \,. \tag{2.3}$$

The factor of 2 is customarily introduced[4] to compensate for the undercounting that otherwise arises [60]. This prescription has the benefit of having an intuitive interpretation — we are

[3] One can also calculate the black hole abundance using peak theory [57–59]. Unlike Press-Schechter, where the overdensity must simply exceed the threshold, peak theory further demands that it be a local maximum. This formalism has been demonstrated to be more appropriate when perturbations exist on multiple scales. As we consider a sharply peaked spectrum, the simpler Press-Schechter prescription suffices for our purposes.

[4] It is unclear whether this factor should still be included when considering asymmetric probability distribution functions, as in the case of non-Gaussianities. We retain it nevertheless since this is an ultimately inconsequential $\mathcal{O}(1)$ effect.

summing over the fraction of regions with a sufficient overdensity to collapse to form a PBH — and a simple implementation. One issue concerns the uncertainty[5] of the collapse threshold, which should in principle depend on the overdensity profile.[6]. Assuming a spherical profile, we expect a perturbation to be able to collapse during radiation domination if the size of the overdensity at maximum expansion exceeds the Jeans length. This led to Carr's original estimate of $\delta_c = c_s^2 = 1/3$ [29], where c_s is the sound speed of density perturbations. A more careful treatment that is applicable for an arbitrary equation of state, w, finds [67]:

$$\delta_c = \frac{3(1+w)}{5+3w} \sin^2\left(\frac{\pi\sqrt{w}}{1+3w}\right) , \tag{2.4}$$

which has been shown to faithfully replicate the results of numerical simulations (provided a sufficiently spherical profile) and yields $\delta_c = 0.414$ during radiation domination. We adopt this value throughout our analysis.

While the coarse-grained density contrast is the proper object to consider when computing the probability of PBH formation, it is often convenient to work directly with the curvature perturbation ζ, since its statistics are more easily computed from underlying inflationary models. When large perturbations exist only on one scale, as is the case for the sharply peaked power spectra we consider, only a minimal amount of error is incurred by making this approximation. On superhorizon scales, ζ is related to the density contrast field by [68]

$$\delta = -\frac{2(1+w)}{5+3w}\left(\frac{1}{aH}\right)^2 e^{-2\zeta}\left(\nabla^2\zeta + \frac{1}{2}(\partial_i\zeta)^2\right) . \tag{2.5}$$

Working to linear[7] order in radiation domination, this simplifies to the Fourier space relation:

$$\delta_k \simeq \frac{4}{9}\left(\frac{k}{aH}\right)^2 \zeta_k , \tag{2.6}$$

which implies that their power spectra, defined for arbitrary Fourier variable f_k via the 2-point function as $\langle f_k f_{k'}\rangle = \frac{2\pi^2}{k^3}\mathcal{P}_f(k)\delta^{(3)}(\vec{k}+\vec{k}')$, are related as

$$\mathcal{P}_\delta(k) \simeq \frac{16}{81}\left(\frac{k}{aH}\right)^4 \mathcal{P}_\zeta(k) . \tag{2.7}$$

Note that at the time of horizon crossing $k \simeq aH$, when a perturbation can collapse to form a black hole, the density contrast and curvature perturbation are linearly related, $\delta \simeq \frac{4}{9}\zeta$. We can then assume that peaks in δ also correspond to peaks in ζ, and work directly with the curvature perturbation. In terms of ζ, the initial abundance in the Press-Schechter formalism reads:

$$\beta \simeq 2\int_{\zeta_c}^{\infty} d\zeta\, P_\zeta[\zeta] , \tag{2.8}$$

[5]It has been demonstrated that a more precise quantity which does away with this uncertainty is the compaction function $\mathcal{C}$, defined as twice the local mass excess over the comoving areal radius [61]. The value of the compaction at its peak is interpreted as the threshold. See also Ref. [62].

[6]Since the overdensity profile is modified in the presence of non-Gaussianities, these can also change the threshold for collapse [63–66] Given the uncertainties involved in these calculations, we take a conservative position and determine δ_c using Eq. (2.4)

[7]A certain degree of non-Gaussianity inevitably arises in the density contrast field due to this nonlinear relation. This implies that even if the statistics of ζ were perfectly Gaussian, those of δ would not be. See, for example, Ref. [68] for discussion.

where the collapse threshold $\zeta_c \simeq \frac{9}{4}\delta_c$ follows from $\sigma_\delta^2 \simeq \frac{16}{81}\sigma_\zeta^2$, since $\mathcal{P} \sim \sigma^2$ for a sharply peaked spectrum. More precisely, the variance of ζ smoothed on the scale $R \simeq (aH)^{-1} \simeq k^{-1}$ can be computed from the power spectrum as [69]

$$\sigma_\zeta^2(R) \equiv \langle\zeta\rangle_R^2 = \int_0^\infty \frac{dk}{k}\tilde{W}^2(k,R)\mathcal{P}_\zeta(k)\,, \tag{2.9}$$

where $\tilde{W}(k,R)$ is the Fourier transform of the (real space) window function used to coarse-grain δ. It is unclear what functional form for the window function most accurately reproduces the actual relation between the PBH abundance and power spectrum, but popular choices in the literature include the (volume normalized) Gaussian, as well as real and k-space top hats. For simplicity, we use the former: $\tilde{W}(k,R) = \exp\left(-k^2R^2/2\right)$, but see Ref. [70] for a discussion of the resultant uncertainties.

Consider the case of a Gaussian distribution $P_\zeta = P_\zeta^G$, where

$$P_\zeta^G = \frac{1}{\sqrt{2\pi}\sigma_\zeta}e^{-\zeta^2/2\sigma_\zeta^2}\,. \tag{2.10}$$

In this case the mass fraction at formation evaluates to

$$\beta = \mathrm{erfc}\left(\frac{\zeta_c}{\sqrt{2}\sigma_\zeta}\right) \simeq \sqrt{\frac{2}{\pi}}\frac{\sigma_\zeta}{\zeta_c}\exp\left(-\frac{\zeta_c^2}{2\sigma_\zeta^2}\right)\,, \tag{2.11}$$

where erfc is the complimentary error function and the second approximation holds for $\zeta_c \gg \sigma_\zeta$, which is generically true for all cases of physical interest. Since the threshold is fixed, the initial abundance is determined solely by the variance of the power spectrum. In order to have $\beta = 10^{-20}$, we see we need $\sigma_\zeta^2 \simeq 0.01$, corresponding to a peak in the power spectrum of $\mathcal{P}_\zeta \sim 0.01$, which is 7 orders of magnitude greater than the value measured on CMB scales. Since the amplification of $\mathcal{P}_\zeta$ needed for PBH formation depends on β only logarithmically, this degree of enhancement is a generic requirement for any non-vanishing initial abundance.

3 Spectral Distortions

The small scales relevant for primordial SMBH formation are well below the angular resolution probed by current CMB measurements. Nevertheless, inhomogeneities on these scales will generate isotropic deviations from the usual blackbody spectrum [71–75]. These deviations are known as spectral distortions and in this context it is useful to distinguish between three characteristic redshift intervals:

- **Thermalization era ($z > 2\times10^6$)**: At high redshifts, Compton scattering $\gamma e \to \gamma e$, double Compton scattering $\gamma e \to \gamma\gamma e$, and Bremsstrahlung $ep \to ep\gamma$ maintain a blackbody spectrum for the photons, and spectral distortions are exponentially suppressed.

- **μ-era ($2\times10^5 < z < 2\times10^6$)**: During this era, photon number changing processes, double Compton scattering and Bremsstrahlung, become ineffective at maintaining a blackbody spectrum. Compton scattering, however, continues to redistribute photon energies to maintain a Bose-Einstein distribution, parameterized by both a temperature, T, and a chemical potential, μ. A μ-distortion refers to a Bose-Einstein distribution with $\mu \neq 0$.

- ***y*-era ($z < 2 \times 10^5$)**: Compton scattering becomes ineffective at redistributing photon energies during this era, so there are no processes to maintain a Bose-Einstein distribution. Spectral distortions that are generated at these redshifts are characterized by a departure from an equilibrium distribution, and often yield so-called y-distortions.[8]

A spectrum with a (positive) y-distortion can be expressed as an average of blackbodies with slightly different temperatures [77–80]. An average of blackbodies with a mean temperature $\bar{T}$ and variance $\bar{T}^2\,\Delta$ will (for $\Delta \ll 1$) be a y-distorted blackbody characterized by the temperature $T = \bar{T}\,(1+\Delta^2)$ and the parameter $y = \Delta^2/2$. y-type distortions can be generated through a variety of mechanisms, including the Compton scattering of CMB photons with a population of electrons with a different temperature. In this paper, we will be interested in y-distortions that are generated through photon diffusion. Limits on such spectral distortions allow us to constrain the amplitude of inhomogeneities on very small scales [81].

μ- and y-type spectral distortions are traditionally quantified in terms of the parameters μ and y, which are related to the fractional increase in energy per photon (relative to a blackbody spectrum with the same number density of photons) [71, 75]:

$$\mu \simeq 1.4\,\frac{\Delta\rho_\gamma}{\rho_\gamma} \qquad \text{and} \qquad y \simeq 0.25\,\frac{\Delta\rho_\gamma}{\rho_\gamma}\ . \tag{3.1}$$

By introducing k-space window functions accounting for the effects of thermalization and dissipation, μ and y can be approximately calculated from the spectrum of density perturbations, P_ζ [75, 79]:

$$\mu \simeq 2.2 \int_{k_{\rm min}}^{\infty} \frac{dk}{k} \mathcal{P}_\zeta(k) \left[\exp\left(-\frac{k}{5400\,{\rm Mpc}^{-1}} \right) - \exp\left(-\left[\frac{k}{31.6\,{\rm Mpc}^{-1}} \right]^2 \right) \right] , \tag{3.2}$$

$$y \simeq 0.4 \int_{k_{\rm min}}^{\infty} \frac{dk}{k} \mathcal{P}_\zeta(k) \exp\left(-\left[\frac{k}{31.6\,{\rm Mpc}^{-1}} \right]^2 \right) , \tag{3.3}$$

where $k_{\rm min} = 1\,{\rm Mpc}^{-1}$.

The strongest existing constraints on spectral distortions come from the COBE/FIRAS instrument, which restricts $|\mu| \lesssim 9.0 \times 10^{-5}$ and $|y| \lesssim 1.5 \times 10^{-5}$ at the 95% C.L. [53, 54]. The standard cosmological model predicts spectral distortions of $\mu \sim 2 \times 10^{-8}$ and $y \sim 10^{-6}$ [82], consistent with current limits. The models of interest in this study have enhanced P_ζ, and thus enhanced μ and y, which can be constrained by CMB measurements.

For concreteness, consider the case of a power spectrum that is sharply peaked at a single scale, $k_{\rm BH}$:

$$\mathcal{P}_\zeta(k) = \sigma_\zeta^2\, k\, \delta(k - k_{\rm BH}). \tag{3.4}$$

Using the delta-function to perform the integral, μ and y become functions of $k_{\rm BH}$ and σ_ζ^2 alone. From the horizon crossing condition $k = aH$, and fact that $H = 1.66\sqrt{g_\star(T)}T^2/M_{\rm Pl}$ during radiation domination, we can relate the wavenumber to the temperature,

$$k_{\rm BH} = 92\,{\rm Mpc}^{-1} \left(\frac{T}{10\,{\rm keV}} \right) \left(\frac{g_\star(T)}{3.36} \right)^{1/2} \left(\frac{3.91}{g_{\star,S}(T)} \right)^{1/3} , \tag{3.5}$$

[8] Technically, the division between the two types of spectral distortions is not entirely unambiguous, and inhomogeneities dissipating around $z \sim 5 \times 10^4$ can give rise to distortions of an intermediate type, whose shape is not simply the sum of μ- and y-type distortions [76].

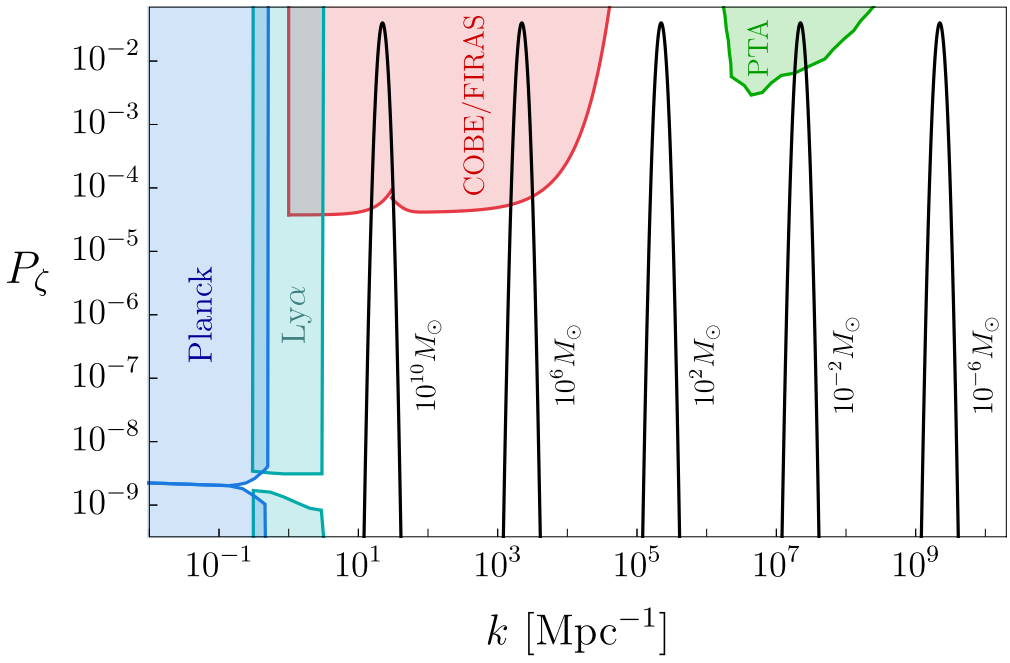

Figure 2. Constraints on the primordial power spectrum $\mathcal{P}_\zeta$ [83] coming from CMB temperature anisotropies (dark blue) [56], Lyman-α forest (light blue) [84], CMB spectral distortions (red) [53, 54], and pulsar timing arrays (green) [85]. The cusp in the COBE/FIRAS excluded region signifies the wavenumber where constraints from μ- and y-type distortions are equally restrictive. Overlaid are illustrative sharply peaked log-normal power spectra resulting in the formation of PBHs with $M_{\rm BH} = 10^{10}, 10^{6}, 10^{2}, 10^{-2}$, and $10^{-6} M_\odot$ and an initial abundance of $\beta = 10^{-20}$, assuming Gaussian statistics for ζ.

which can then be related to the horizon mass using Eq. (1.3) to estimate the mass of the resulting black hole:

$$M_{\rm BH} \simeq 5 \times 10^{8}\, M_\odot \left(\frac{92\,{\rm Mpc}^{-1}}{k_{\rm BH}}\right)^{2} \left(\frac{\gamma}{0.2}\right) \left(\frac{g_\star(T)}{3.36}\right)^{1/2} \left(\frac{3.91}{g_{\star,S}(T)}\right)^{2/3} . \tag{3.6}$$

For the sharply peaked spectrum of Eq. (3.4), adopting $\gamma = 0.2$, and for black holes in the mass range of interest, the μ- and y-parameters can be written as

$$\mu \simeq 2.2\sigma_\zeta^2 \left\{ \exp\left[-\left(\frac{1.5\times 10^{5}\, M_\odot}{M_{\rm BH}}\right)^{1/2}\right] - \exp\left[-\left(\frac{4.5\times 10^{9}\, M_\odot}{M_{\rm BH}}\right)\right] \right\}, \tag{3.7}$$

$$y \simeq 0.4\sigma_\zeta^2 \exp\left[-\left(\frac{4.5\times 10^{9}\, M_\odot}{M_{\rm BH}}\right)\right] . \tag{3.8}$$

Note that these results should also hold, for example, in the case of a log-normal spectrum of sufficiently narrow width.

In Eqs. (3.7) and (3.8), we can identify the impact of the various eras described earlier in this section. In particular, for $M_{\rm BH} \ll 1.5\times 10^{5}\, M_\odot$ (corresponding to $k_{\rm BH} \gg 5400/{\rm Mpc}$), the black holes are formed during the thermalization era, and both μ- and y-type spectral distortions are suppressed. For $1.5\times 10^{5}\, M_\odot \ll M_{\rm BH} \ll 4.5\times 10^{9}\, M_\odot$ ($31.6/{\rm Mpc} \lesssim k_{\rm BH} \lesssim$

5400/Mpc), the black holes are forming during the μ-era, leading primarily to μ-type spectral distortions. Larger black holes form later, yielding primarily y-type spectral distortions.

We can use Eqs. (3.7) and (3.8) to quickly estimate whether a scenario featuring primordial SMBHs is consistent with spectral distortion constraints. [9] Recall that, for the case of Gaussian statistics, a value of $\sigma_\zeta^2 \gtrsim 10^{-2}$ is required in order to obtain a non-negligible abundance of PBHs. For such large values of σ_ζ^2, spectral distortions exclude all black holes masses $M_{\rm BH} \gtrsim \text{few} \times 10^2 M_\odot$. This conclusion is consistent with Fig. 2, where we compare the bounds from COBE/FIRAS with the power spectra predicted for several values of $M_{\rm BH}$. Therefore, the existence of a non-negligible abundance of primordial SMBHs requires the presence of significant non-Gaussianities in the distribution of the primordial curvature perturbations.

4 Departures from Gaussianity

For Gaussian density perturbations, constraints from spectral distortions severely limit the abundance of primordial SMBHs that could have formed in the early universe. In this case, the variance must be small in order to limit spectral distortions, while a large variance is required to generate a non-negligible abundance of PBHs. This tension could be resolved, however, if the distribution of curvature perturbations features a heavier tail than that of a Gaussian. Such non-Gaussianities thus potentially allow primordial SMBHs to form without necessarily violating spectral distortion constraints.

Fortunately, the distribution of primordial density perturbations is generically predicted to be non-Gaussian. Firstly, there is intrinsic non-Gaussianity that arises from the non-linear mapping between the curvature perturbation ζ and the density contrast δ, as can be seen in Eq. (2.5). Thus, even if the probability distribution function for ζ were exactly Gaussian, the distribution in δ would not be. Secondly, and more crucially, large departures from Gaussianity are generically found in models which produce a local enhancement in the primordial power spectrum [68].

To quantify the degree of non-Gaussianity that would be required to generate primordial SMBHs without violating spectral distortion constraints, it is instructive to consider a class of probability distribution functions of the form [87]

$$P_\delta^{(n)} = \frac{1}{2\sqrt{2}\,\sigma_0\,\Gamma\left(1+\frac{1}{n}\right)} \exp\left[-\left(\frac{|\delta|}{\sqrt{2}\sigma_0}\right)^n\right], \tag{4.1}$$

where n parameterizes the heaviness of the distribution's tail. The variance of the density contrast is set by the second moment of the distribution:

$$\sigma_\delta^2(\sigma_0) \equiv \int_{-\infty}^{\infty} d\delta\, \delta^2\, P_\delta^{(n)} = \frac{\sigma_0^2\,\Gamma\left(1+\frac{3}{n}\right)}{3\Gamma\left(1+\frac{1}{n}\right)}\,. \tag{4.2}$$

Note that for $n = 2$, this reduces to the Gaussian form of Eq. (2.10) with $\sigma_0^2 = \sigma_\delta^2$. For $n = 1$ the tail falls off exponentially, while for $0 < n < 1$ it falls off even more slowly; we will refer to this class of distributions with $n < 1$ as "heavy-tailed."[10]

In Fig. 3, we show the shape of this class of probability distributions for various choices of n. As expected, we see that smaller n gives rise to heavier tails. This raises the question of

[9] The validity of the formulas used in this paper has been explored in Ref. [86]. We believe they are valid across in our regime of interest, but may differ at most by order one factors for large amplitude inhomogeneities.

[10] Formally, the probability distribution P_x of a random variable x is said to be "heavy" if its tail is not exponentially bounded, $\lim_{x\to\infty} e^{\lambda x}\bar{F}(x) = \infty\, \forall\, \lambda > 0$, where $\bar{F}(x) = \int_x^\infty dx'\, P_x(x')$.

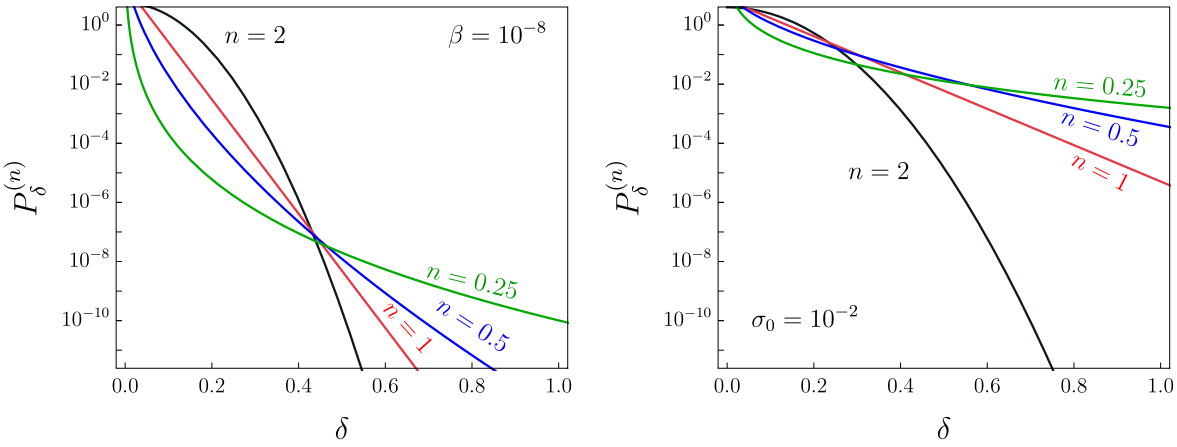

Figure 3. Probability distribution functions Eq. 4.1 for various choices of n at fixed β (left) and fixed variance σ^2 (right). We see that smaller n corresponds to heavier-tailed distributions.

how small n must be in order to efficiently form primordial SMBHs while keeping the peak of the power spectrum within bounds of spectral distortions, $\mathcal{P}_\zeta \lesssim 10^{-4}$. In Fig. 4, we plot the maximum PBH mass fraction at formation $\beta_{\rm max}$, for a variance that saturates the spectral distortion constraints from COBE/FIRAS. Note that to generate a present day abundance of $\Omega_{\rm BH} \gtrsim 10^{-20}$ with $M_{\rm BH} \lesssim 10^{11} M_\odot$, we need a heavy tail with $n \lesssim 0.6$.

We now turn to the question of what inflationary models could yield such dramatic departures from Gaussianity. In the context of single-field inflation, Refs. [88–91] perturbatively studied the local non-Gaussianity that arises in models which deviate from the slow-roll attractor, as in ultra-slow-roll inflation. Going beyond perturbation theory, Refs. [37, 42] use the δN formalism [92–97] to compute the non-perturbative distribution of curvature perturbations. For inflaton potentials with a small step or bump-like feature that induces a period of off-attractor behavior, these studies find that the tail of the distribution can become exponential, without inducing any significant non-Gaussianities in the perturbative regime [37]. This result highlights the fact that perturbative measures of non-Gaussianity are not generally adequate to describe the large, rare fluctuations that lead to PBH formation. Finally, many of the mechanisms for enhancing local curvature perturbations rely on a temporary reduction in the inflaton's velocity. When the slow-roll classical drift vanishes, the field dynamics can receive large corrections from quantum diffusion, and the stochastic inflationary formalism [93, 98] may be necessary for a proper description of the dynamics. Combining this with the δN formalism [99], a number of studies [38, 40, 41, 100, 101] have found that prominent exponential tails arise generically from quantum diffusion.

While many single-field models have been found to yield exponential tails, there is currently no known model which generates a heavier-tailed distribution.[11] However, as shown in Fig. 4, a heavy tail $P_\delta \sim \exp\left(-|\delta|^n\right)$ with $n \lesssim 0.6$ is needed to yield a non-negligible population of primordial SMBHs while satisfying bounds from CMB spectral distortions. While it is unclear whether primordial SMBHs can appreciably form in any viable single-field models, the necessary heavy tails can arise in certain multi-field scenarios. As we show in the next

[11] Ref. [102] interprets the NANOGrav signal as evidence of PBH mergers with $M_{\rm BH} \sim 10^{11} - 10^{12} M_\odot$, and claims that μ-distortion constraints can be overcome for sufficiently non-Gaussian single-field models. However they make no reference to y-type distortions, which are more constraining for this mass range, and which we have verified rule out this single-field scenario for any non-negligible abundance.

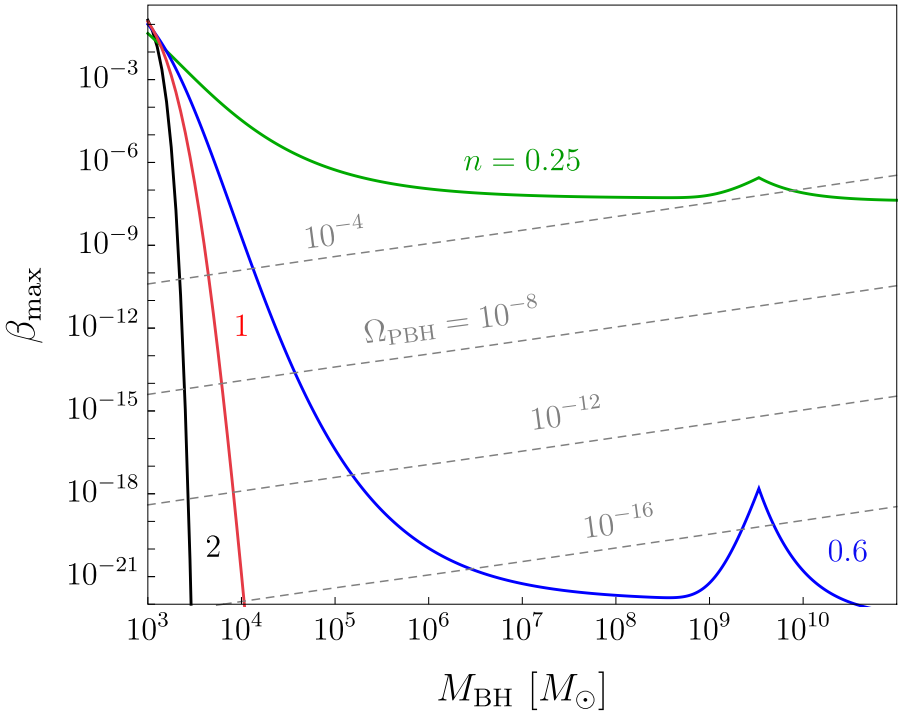

Figure 4. The maximum primordial black hole mass fraction at formation $\beta_{\rm max}$ as a function of mass $M_{\rm BH}$ for a value of the variance σ_ζ^2 that saturates the spectral distortion constraints from COBE/FIRAS, as estimated according to Eq. (3.7). We assume the distribution function given in Eq. (4.1) and consider Gaussian ($n = 2$, black), exponential ($n = 1$, red), and power law ($n = 0.6$ blue, $n = 0.25$ green) behavior in the tail. Note that the cusps which appear near $M_{\rm BH} \sim 3 \times 10^9\, M_\odot$ correspond to the value of $M_{\rm BH}$ at which μ- and y-type spectral distortions are equally restrictive. Contours of constant $\Omega_{\rm BH}$, as computed using Eq. (2.2), are shown in dashed gray.

section, the non-minimal curvaton model supplemented with self-interactions can generate such a heavy-tailed distribution.

5 Standard Curvaton Scenario

Curvaton models introduce a second light, unstable spectator field that is present during inflation and that is responsible for generating the dominant contribution to the primordial curvature perturbations [103–105]. The perturbations of the curvaton are initially isocurvature, but become adiabatic upon curvaton decay sometime after inflation ends [106]. Due to the non-linearity inherent in this transfer, the full perturbation ζ can become quite non-Gaussian. In particular, when the curvaton is still very subdominant at decay, the inefficient conversion can yield a very heavy-tailed distribution for ζ.

Non-Gaussianity in the curvaton model was first investigated using the δN formalism in Ref. [107]. A follow-up study [49] introduced a minimal modification which produces a peak in the spectrum, with implications for PBH formation. As we will see, the standard curvaton model with only a quadratic potential cannot produce sufficient non-Gaussianity to generate a non-negligible abundance of SMBHs without violating spectral distortions constraints.

5.1 Curvaton Cosmology

We begin by reviewing the calculation of the curvature perturbation ζ and its statistics in the standard curvaton scenario [107], for which the total potential is

$$V(\phi, \chi) = V_\phi(\phi) + V_\chi(\chi)\,, \tag{5.1}$$

where V_ϕ is the unspecified potential of the inflaton ϕ, and $V_\chi = m_\chi^2\chi^2/2$ is the quadratic potential of the curvaton χ. The curvaton mass is required to be light, satisfying $m_\chi \ll H$ throughout inflation, such that quantum perturbations are the dominant influence on its evolution. This also implies that the background field $\bar{\chi}$ will remain effectively fixed at some initial value $\bar{\chi}_*$ during inflation, where a star denotes the value of quantities at horizon exit. For the curvaton energy density to remain subdominant throughout inflation, we demand $\bar{\chi}_* \ll \sqrt{2V_\phi/m_\chi^2}$. Just like the inflaton, the curvaton receives perturbations $\delta\chi_* \simeq H_*/2\pi$ set by the Hubble rate at horizon exit H_*. Since the curvaton is a weakly coupled field, we expect the perturbations $\delta\chi_*$ to be described by a Gaussian random field. Thus we can write the curvaton at horizon exit as the sum of a background field and a linear perturbation, with no higher order terms:

$$\chi_* = \bar{\chi}_* + \delta\chi_*\,. \tag{5.2}$$

The goal of this section will be to relate these initial Gaussian field perturbations to the total curvature perturbation ζ via some mapping $\zeta = f(\delta\chi_*)$. This will be the key to constructing the probability distribution function for ζ, since the statistics of a non-Gaussian variable are completely determined by the statistics of a Gaussian reference variable when the mapping between them is specified.

When inflation ends and the inflaton decays, the universe enters into an era of radiation domination, with $\rho_R \sim a^{-4}$. At this point, the curvaton energy density is subdominant and its fluctuations are still isocurvature in nature. As the Hubble rate decreases, it eventually drops below m_χ, causing the curvaton to start oscillating about the minimum of its potential. We denote the field value at which this occurs by $\bar{\chi}_0$. During this oscillating phase, the curvaton redshifts like matter with $\rho_\chi \propto a^{-3}$ and its energy density grows linearly relative to radiation. Finally, when $H \sim \tau^{-1}$, where τ is the χ lifetime, the curvaton decays to radiation and its isocurvature perturbations become adiabatic perturbations, assuming the decay products thermalize with the existing radiation.

5.2 The δN Formalism

To calculate the distribution of the curvature perturbations in this model, we employ the δN formalism [92–97, 108], which we review in Appendix A. This technique identifies ζ on large scales ($k \ll aH$) with the variation of inflationary e-folds across Hubble patches and non-perturbatively captures its non-Gaussianities. The δN formalism was first used to study non-Gaussianity in curvaton models in Ref. [107, 109]. On a general hypersurface of uniform curvaton density, the conserved curvaton curvature perturbation ζ_χ is [96, 109]

$$\zeta_\chi(t, \vec{x}) = \delta N(t, \vec{x}) + \frac{1}{3}\ln\left(\frac{\rho_\chi(t, \vec{x})}{\bar{\rho}_\chi(t)}\right)\,, \tag{5.3}$$

where $\delta N(t, \vec{x})$ is the perturbed number of e-folds, $\rho_\chi(t, \vec{x})$ is the χ energy density, and $\bar{\rho}_\chi(t)$ is its background value. In spatially flat slicing, this becomes

$$\zeta_\chi(t, \vec{x}) = \frac{1}{3}\ln\left(\frac{\rho_\chi(t, \vec{x})}{\bar{\rho}_\chi(t)}\right)\,, \tag{5.4}$$

and the curvaton energy density can be written as

$$\rho_\chi(t,\vec{x}) = e^{3\zeta_\chi(t,\vec{x})}\,\bar{\rho}_\chi(t)\,. \tag{5.5}$$

In uniform total density slicing, Eq. (5.3) becomes

$$\zeta_\chi(t,\vec{x}) = \zeta + \frac{1}{3}\ln\left(\frac{\rho_\chi^{(u)}(t,\vec{x})}{\bar{\rho}_\chi^{(u)}(t)}\right)\,, \tag{5.6}$$

where ζ is the total curvature perturbation.[12] Since ζ and ζ_χ are gauge invariant quantities, Eq. (5.5) can be equated with Eq. (5.6) to yield

$$\rho_\chi^{(u)}(t,\vec{x}) = e^{3(\zeta_\chi-\zeta)}\bar{\rho}_\chi^{(u)}(t)\,. \tag{5.7}$$

A similar treatment for the radiation energy density in uniform total density slicing gives

$$\rho_R^{(u)}(t,\vec{x}) = e^{4(\zeta_R-\zeta)}\bar{\rho}_R^{(u)}(t) \simeq e^{-4\zeta}\bar{\rho}_R^{(u)}(t)\,, \tag{5.8}$$

where we have assumed for simplicity that the main contribution to the curvature perturbation comes from the curvaton. In order to derive analytic results, we work in the instantaneous decay approximation such that the curvaton decays when $H = \tau^{-1}$, where τ is the curvaton lifetime. On a uniform total density slice at $t = \tau$, the energy densities satisfy

$$\rho_R^{(u)}(\tau,\vec{x}) + \rho_\chi^{(u)}(\tau,\vec{x}) = \bar{\rho}^{(u)}(\tau)\,, \tag{5.9}$$

where $\bar{\rho}^{(u)} = \bar{\rho}_R^{(u)} + \bar{\rho}_\chi^{(u)}$ is the total homogeneous energy density. Substituting Eqs. (5.7) and (5.8), this becomes a 4^{th} degree algebraic equation for ζ at τ:

$$e^{4\zeta} - \left(e^{3\zeta_\chi}\,\Omega_{\chi,\tau}\right)e^{\zeta} + (\Omega_{\chi,\tau} - 1) = 0\,. \tag{5.10}$$

Alternatively, it is customary to introduce the parameter r_τ, defined as [103]:

$$r_\tau = \frac{3\Omega_{\chi,\tau}}{4-\Omega_{\chi,\tau}} = \left.\frac{3\bar{\rho}_\chi^{(u)}}{3\bar{\rho}_\chi^{(u)} + 4\bar{\rho}_R^{(u)}}\right|_\tau\,, \tag{5.11}$$

in terms of which the equation for ζ becomes:

$$e^{4\zeta} - \frac{4r_\tau}{3+r_\tau}\left(e^{3\zeta_\chi}\right)e^{\zeta} + \frac{3r_\tau - 3}{3+r_\tau} = 0\,. \tag{5.12}$$

The general solution is

$$\zeta = \ln X\,,\quad X = \frac{B^{1/2} + \sqrt{Ar_\tau B^{-1/2} - B}}{(3+r_\tau)^{1/3}}\,, \tag{5.13}$$

where $A = e^{3\zeta_\chi}$ and we have defined

$$B = \frac{1}{2}\left[C^{1/3} + (r_\tau - 1)(3+r_\tau)^{1/3}C^{-1/3}\right] \tag{5.14}$$

$$C = (Ar_\tau)^2 + \sqrt{(Ar_\tau)^4 + (3+r_\tau)(1-r_\tau)^3}\,. \tag{5.15}$$

This gives the mapping $\zeta = \ln[X(\zeta_\chi)]$ between ζ and ζ_χ.

[12] Note that this generically has non-vanishing mean, $\langle\zeta\rangle \neq 0$, and so when we later consider PBH formation, we will have to define a physical $\zeta_{\rm phys} \equiv \zeta - \langle\zeta\rangle$ [49]. The expectation value $\langle\zeta\rangle$ can be computed using the Gaussian P_{δ_χ} as $\langle\zeta\rangle = \int d\delta_\chi\,\zeta\,P_{\delta_\chi}$, with ζ expressed as a function of δ_χ given in Eq. (5.13).

5.3 Calculating the Probability Distribution

Finally, to obtain ζ_χ in terms of $\delta\chi_*$, we return to Eq. (5.4), which gave the curvature perturbation in spatially flat slicing as a function of perturbed and background energy densities. For the simple quadratic potential of this model, we have $\rho_\chi(t,\vec{x}) = m_\chi^2\chi^2/2$. Expanding $\chi(t,\vec{x}) = \bar{\chi}(t) + \delta\chi(t,\vec{x})$, we can write this as

$$\rho_\chi(t,\vec{x}) = \frac{1}{2}m_\chi^2\bar{\chi}^2\left(1+\frac{\delta\chi}{\bar{\chi}}\right)^2 = \bar{\rho}_\chi(t)(1+\delta_\chi)^2\,, \tag{5.16}$$

where $\delta_\chi = \delta\chi/\bar{\chi}$ is the curvaton contrast in spatially flat slicing. Comparing with $\rho_\chi = e^{3\zeta_\chi}\bar{\rho}_\chi$, we see we should identify $e^{3\zeta_\chi} = (1+\delta_\chi)^2$. Finally in order to relate the contrast δ_χ to its value at horizon exit, consider the equations of motion for χ and the perturbation $\delta\chi$:

$$\frac{d^2\bar{\chi}}{dt^2} + 3H\frac{d\bar{\chi}}{dt} + m_\chi^2\bar{\chi} = 0\,, \tag{5.17a}$$

$$\frac{d^2}{dt^2}(\delta\chi) + 3H\frac{d}{dt}(\delta\chi) + \left(\frac{k^2}{a^2}+m_\chi^2\right)\delta\chi = 0\,. \tag{5.17b}$$

On superhorizon scales $k \ll aH$ is negligible and so these reduce to the same equation. This implies $\delta\chi \sim \bar{\chi}$, such that $\delta\chi/\bar{\chi} = \delta\chi_*/\bar{\chi}_*$ and

$$A = e^{3\zeta_\chi} = (1+\delta_\chi)^2 = \left(1+\frac{\delta\chi_*}{\bar{\chi}_*}\right)^2\,. \tag{5.18}$$

Combining with Eq. (5.13), we obtain the desired mapping between ζ and the Gaussian initial field perturbations $\delta\chi_*$. We can now use probability conservation to write

$$P_\zeta[\zeta] = P_{\delta_\chi}\left[\delta_\chi^+(\zeta)\right]\left|\frac{d\delta_\chi^+}{d\zeta}\right| + P_{\delta_\chi}\left[\delta_\chi^-(\zeta)\right]\left|\frac{d\delta_\chi^-}{d\zeta}\right|\,, \tag{5.19}$$

where P_{δ_χ} is fully determined by the Gaussian variance σ_0^2 and the roots $\delta_\chi^\pm(\zeta)$ satisfy

$$\delta_\chi^\pm = -1 \pm \sqrt{\left(\frac{3+r_\tau}{4r_\tau}\right)e^{3\zeta} + \left(\frac{3r_\tau-3}{4r_\tau}\right)e^{-\zeta}}\,, \tag{5.20}$$

which arise from solving Eq. (5.12) and substituting Eq. (5.18). In Fig. (5), we plot the probability distribution for the curvature perturbation as given by Eq. (5.19) for a few choices of r_τ, which controls the heaviness of the tail.

6 Heavy Tails and Primordial Black Holes in Curvaton Models

Viably forming an appreciable number of primordial SMBHs requires both amplified power on small scales and a departure from Gaussianity. These goals can be achieved with two additional ingredients:

- **Enhanced Power:** One mechanism for enhancing the power spectrum is to introduce a non-canonical kinetic term for the curvaton, which depends on the inflaton's field value [49]. In Sec. 6.1 we review this scenario and calculate the power spectrum that results from such a kinetic term.

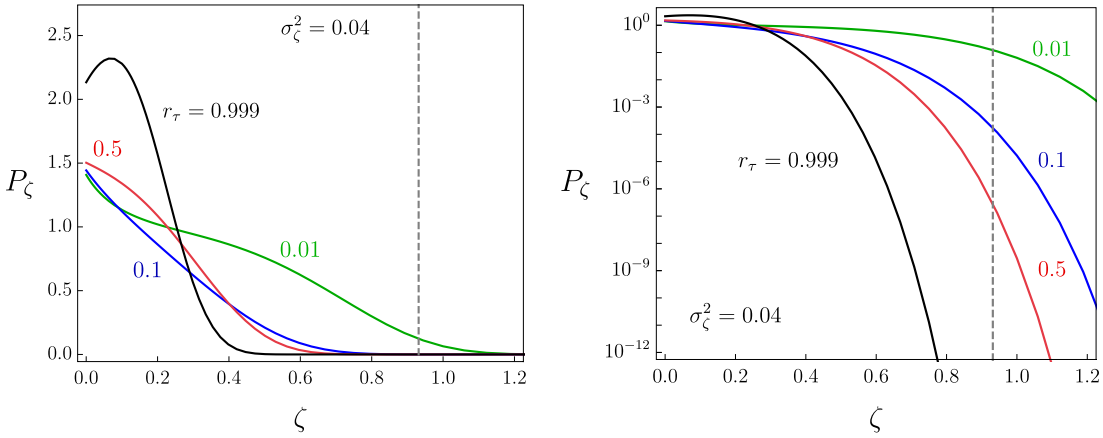

Figure 5. The probability distribution function for the curvature perturbation ζ as given by Eq. (5.19) for various choices of r_τ. The vertical dashed line corresponds to the threshold value for collapse ζ_c, and the PBH mass fraction β is obtained by integrating beyond this threshold. We see that a smaller r_τ corresponds to a heavier-tailed distribution, leading to a larger PBH abundance. Note that the reference value $\sigma_\zeta^2 = 0.04$ is chosen to illustrate the heaviness of the tail as r_τ is varied, but the minimal scenario presented in Sec. 5 cannot realize such a large value without violating the observational limits on the power spectrum shown in Fig. 2.

- **Large Non-Gaussianity:** The non-Gaussianity in a curvaton model can be amplified through self-interactions, which lead to non-linear growth of χ perturbations between horizon exit and the onset of curvaton oscillations. While such interactions were studied perturbatively in Refs. [110–114], in Sec. 6.2 we go beyond these works to compute the non-perturbative probability distribution function.

A curvaton model with these additional ingredients can generate an appreciable SMBH population from the direct collapse of inflationary perturbations.

6.1 Non-Minimal Curvaton Scenario

The minimal curvaton model described in Sec. 5 provides non-Gaussian statistics, but does not amplify $\mathcal{P}_\zeta$. This deficiency can be remedied with a non-canonical kinetic term[13] for the curvaton [49]:

$$\mathcal{L} \supset \frac{1}{2} f(\phi)^2 (\partial\chi)^2 \,. \tag{6.1}$$

If $f(\phi)$ is chosen such that this kinetic term is suppressed at field values $\phi = \phi_*$, the power spectrum will be enhanced on scales corresponding to the horizon size at ϕ_*. For concreteness, consider the evolution of the inflaton and curvaton governed by the following system of equations:

$$\ddot{\phi} + 3H\dot{\phi} + V'(\phi) = f f' \dot{\bar{\chi}}^2 \simeq 0 \,, \quad \ddot{\bar{\chi}} + \left(3H + \frac{2f'}{f}\dot{\phi}\right)\dot{\bar{\chi}} + \frac{m_\chi^2}{f^2}\bar{\chi} = 0 \,, \tag{6.2}$$

where $f' \equiv \partial_\phi f$ and the source term of the first equation is negligible until the curvaton begins to oscillate. Similarly, the curvaton perturbation evolves according to

$$\frac{d^2}{dt^2}(\delta\chi) + \left(3H + \frac{2f'}{f}\dot{\phi}\right)\frac{d}{dt}(\delta\chi) + \left(\frac{k^2}{a^2} + \frac{m_\chi^2}{f^2}\right)\delta\chi \simeq 0 \,, \tag{6.3}$$

[13] Such a term naturally arises in many dilatonic and axionic models of inflation [115].

which, to leading order, can be simplified inside the horizon, $k \gg aH$, to yield

$$\frac{d^2}{dt^2}(f\delta\chi) + \frac{k^2}{a^2}(f\delta\chi) \simeq 0\,, \tag{6.4}$$

whose solution can be written as

$$\delta\chi \simeq \frac{1}{\sqrt{2k}\,af} \exp\left(-ik\int \frac{dt}{a}\right), \tag{6.5}$$

which establishes the initial conditions in the adiabatic vacuum. As in Sec. 5, on superhorizon scales, $k \ll aH$, $\bar{\chi}$ and $\delta\chi$ evolve according to the same equation, so their solutions have the same functional form for all $t > t_*$:

$$\frac{\delta\chi}{\bar{\chi}} = \frac{\delta\chi_*}{\bar{\chi}_*} \simeq \frac{H_*}{\sqrt{2k^3 f(\phi_*)}\bar{\chi}_*}\,, \tag{6.6}$$

where $k = a(t_*)H(t_\star)$. Using Eq. (6.6), the power spectrum for δ_χ becomes

$$\mathcal{P}_{\delta_\chi}(k) = \frac{k^3}{2\pi^2}\left|\frac{\delta\chi_k}{\bar{\chi}}\right|^2 = \frac{1}{\bar{\chi}_*^2}\left(\frac{H_*}{2\pi f(\phi_*)}\right)^2\,, \tag{6.7}$$

so, if $f(\phi)$ is chosen to have a dip at ϕ_*, corresponding to $k_* = k_{\rm BH}$, $\mathcal{P}_{\delta_\chi}$ will exhibit a peak at $k_{\rm BH}$. However, for modes far away from $k_{\rm BH}$, $f(\phi_*) \approx 1$, recovering the nearly scale-invariant spectrum required for consistency with CMB observations on larger scales. Assuming $f(\phi)$ has such a localized feature, combining Eqs. (5.19), (6.7), and (2.8), the PBH abundance becomes

$$\beta = 2\int_{\delta^+_{\chi,c}}^{\infty} d\delta_\chi\, P_{\delta_\chi}[\delta_\chi] + 2\int_{-\infty}^{\delta^-_{\chi,c}} d\delta_\chi\, P_{\delta_\chi}[\delta_\chi] = \mathrm{erfc}\left(\frac{\delta^+_{\chi,c}}{\sqrt{2}\sigma_0}\right) + \mathrm{erfc}\left(\frac{|\delta^-_{\chi,c}|}{\sqrt{2}\sigma_0}\right)\,, \tag{6.8}$$

where $\delta^\pm_{\chi,c} = \delta^\pm_\chi(\zeta_c)$ are the roots of Eq. (5.20) evaluated at the threshold.

Using Eq. (3.7), we obtain the maximum value of β consistent with spectral distortion constraints.[14] The degree of non-Gaussianity in this scenario is governed by r_τ, as defined in Eq. (5.11). In the $r_\tau \to 1$ limit, the curvaton dominates the energy density prior to its decay, so the relation between ζ and ζ_χ from Eq. (5.12) is approximately linear. Thus, in this regime, we expect only a small departure from Gaussianity. In the opposite regime[15] that the curvaton is still very subdominant when it decays ($r_\tau \ll 1$), the relation between ζ and ζ_χ is highly non-linear, and so the degree of non-Gaussianity is large. This is reflected in Figs. 5 and 6. Clearly this scenario is incapable of producing primordial SMBHs while satisfying spectral distortion constraints.

[14] Note that the variance σ_ζ^2 corresponds to the physical curvature perturbation, $\sigma_\zeta^2 = \langle\zeta^2_{\rm phys}\rangle = \langle\zeta^2\rangle - \langle\zeta\rangle^2$, which can be computed from $\zeta(\delta_\chi)$ in Eq. (5.13) as $\sigma_\zeta^2 = \int d\delta_\chi\, \zeta^2\, P_{\delta_\chi} - \left(\int d\delta_\chi\, \zeta\, P_{\delta_\chi}\right)^2$.

[15] It may seem counterintuitive that a very subdominant curvaton can still generate the curvature perturbation. The key is that because the curvaton is subdominant during inflation, its perturbations from quantum fluctuations are large relative to the background field value. Ref. [116] finds that a subdominant curvaton can still viably produce the curvature perturbation provided $r_\tau \gtrsim 10^{-3}$.

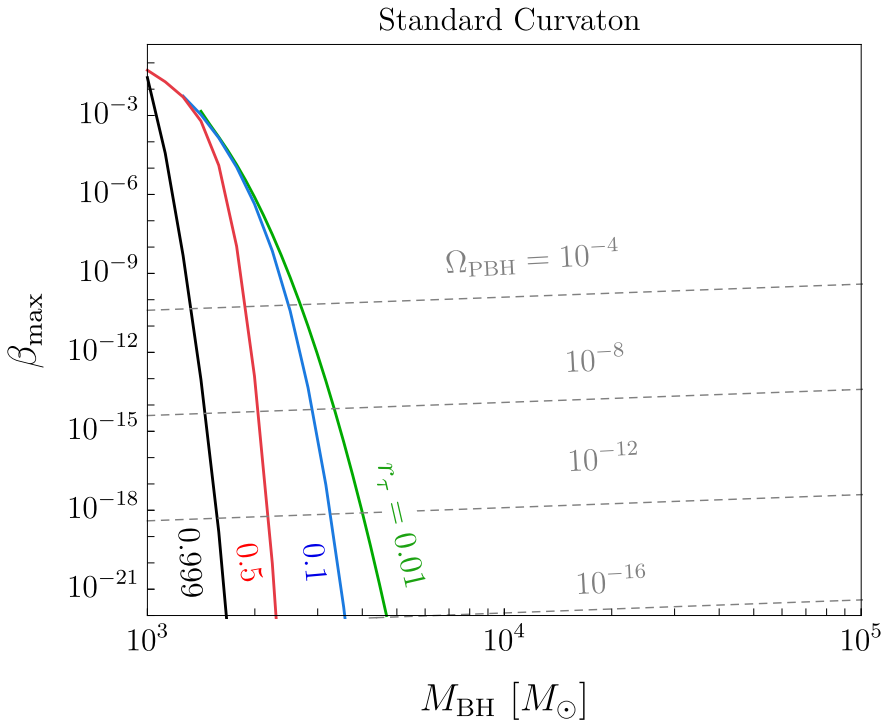

Figure 6. The maximal PBH mass fraction at formation $\beta_{\rm max}$ in the standard curvaton scenario for σ_ζ^2 subject to spectral distortion constraints for various choices of r_τ from Eq. (5.11)

6.2 Self-Interacting Curvaton Scenario

Introducing curvaton self-interactions allows for non-linear δ_χ between horizon exit and the onset of oscillations, leading to even more dramatic departures from Gaussianity.[16] The effects of weak self-interactions in curvaton models were first investigated in Refs. [110–114]. However, these studies restricted themselves to computing the non-linearity parameters $f_{\rm NL}$ and $g_{\rm NL}$, which do not capture the non-perturbative statistics in the tail of the distribution. By employing the δN formalism, we extend these studies to compute the full probability distribution for ζ.

We now allow the curvaton potential to be an arbitrary well-defined function of χ. In our setup, at $t = t_{\rm int}$, corresponding to $V'(\chi_*) \sim H$, χ begins rolling towards the minimum of its potential and its energy density is initially dominated by the interaction terms. At a later time $t = t_0 > t_{\rm int}$, the interaction terms become subdominant, and the curvaton mass term drives field evolution, resulting in matter-like scaling, $\rho_\chi \propto a^{-3}$. Note that with self-interactions, the curvaton energy density generically falls off faster than in the quadratic case, resulting in a smaller r_τ at the time of decay.

Recall that in the case of the quadratic potential, the curvaton density contrast δ_χ remained constant after horizon exit since the background field $\bar{\chi}$ and perturbation $\delta\chi$ obeyed the same equation of motion, shown in Eq. (5.17). This led to $\delta\chi/\bar{\chi} = \delta\chi_*/\bar{\chi}_*$, which allowed δ_χ to be used as a Gaussian reference variable. Upon introducing interactions this is no longer the case, as δ_χ evolves non-trivially between $t_{\rm osc}$ and curvaton decay at $t = \tau$. In the regime,

[16] This scenario is also physically well-motivated since the curvaton needs to decay for the isocurvature perturbations to be converted to adiabatic perturbations.

the equation of motion for the perturbation is:

$$\frac{d^2}{dt^2}(\delta\chi) + 3H\frac{d}{dt}(\delta\chi) + V''_\chi \delta\chi = 0\,, \tag{6.9}$$

where it is understood that the second derivative of the potential should be evaluated at the background field value.

A natural choice of Gaussian reference variable is the initial curvaton perturbation $\delta\chi_*$, which can be related to the ζ_χ by first solving Eq. (6.9) along with the equation for the background field $\bar{\chi}$, computing the total and background energy densities at decay, and finally applying Eq. (5.4). The resulting $\delta\chi^i_* = g_i(\zeta_\chi)$ can then be mapped onto the total curvature perturbation ζ via Eq. (5.12), since the relationship between ζ_χ and ζ is unchanged in the presence of χ self-interactions. Although an exact solution requires the use of numerical techniques, an approximate relation can be derived in the limit of weak interactions.

We are interested in the relation between $\delta\chi_*$ and ζ_χ at the time of curvaton decay. For χ values sufficiently close to the minimum of its potential, the potential is approximately quadratic, and the energy density is

$$\rho_\chi \simeq \frac{1}{2}m_\chi^2\chi_0^2\,, \tag{6.10}$$

where χ_0 is the amplitude at the onset of oscillations. Since non-linear evolution takes place between horizon exit and oscillation, this initial amplitude is a function of initial field value χ_*). In terms of background field values $\bar{\chi}_0 \equiv \chi_0(\bar{\chi}_*)$, this can be expanded as:

$$\chi_0 = \bar{\chi}_0 + \sum_{n=1}\frac{1}{n!}\bar{\chi}_0^{(n)}\delta\chi_*^n \quad , \quad \bar{\chi}_0^{(n)} \equiv \left.\frac{\partial^n\chi_0}{\partial\chi_*^n}\right|_{\chi=\bar{\chi}_*}, \tag{6.11}$$

and the energy density can then be written as:

$$\rho_\chi \simeq \bar{\rho}_\chi\left[1 + \frac{1}{\bar{\chi}_0}\sum_{n=1}\frac{1}{n!}\bar{\chi}_0^{(n)}\delta\chi_*^n\right]^2, \tag{6.12}$$

where $\bar{\rho}_\chi = \frac{1}{2}m_\chi^2\bar{\chi}_0^2$. Comparing with Eq. (5.4), the bracketed quantity is identified with $e^{3\zeta_\chi}$. Then also expanding

$$\zeta_\chi = \zeta_{\chi,1} + \sum_{n=2}^{\infty}\frac{1}{n!}\zeta_{\chi,n} \quad , \tag{6.13}$$

we can write to leading order:

$$\zeta_\chi(\delta\chi_*) = \frac{2}{3}\left(\frac{\bar{\chi}_0'}{\bar{\chi}_0}\right)\delta\chi_* + \frac{1}{3}\left(\frac{\bar{\chi}_0\bar{\chi}_0''}{\bar{\chi}_0'^2}\right)\left(\frac{\bar{\chi}_0'}{\bar{\chi}_0}\right)^2\delta\chi_*^2 + \frac{2}{9}\left(1 - \frac{3}{2}\frac{\bar{\chi}_0\bar{\chi}_0''}{\bar{\chi}_0'^2} + \frac{1}{2}\frac{\bar{\chi}_0^2\bar{\chi}_0'''}{\bar{\chi}_0'^3}\right)\left(\frac{\bar{\chi}_0'}{\bar{\chi}_0}\right)^3\delta\chi_*^3\,, \tag{6.14}$$

which can then be substituted into Eq. (5.13) to obtain ζ as a function of the Gaussian reference variable $\delta\chi_*$. It is also possible to invert this mapping to obtain the roots $g_i(\zeta) = \delta\chi^i_*(\zeta)$. The probability distribution is then:

$$P_\zeta[\zeta] = \sum_j\left|\frac{g_j(\zeta)}{d\zeta}\right|P_{\delta\chi_*}[g_j(\zeta)]\,, \tag{6.15}$$

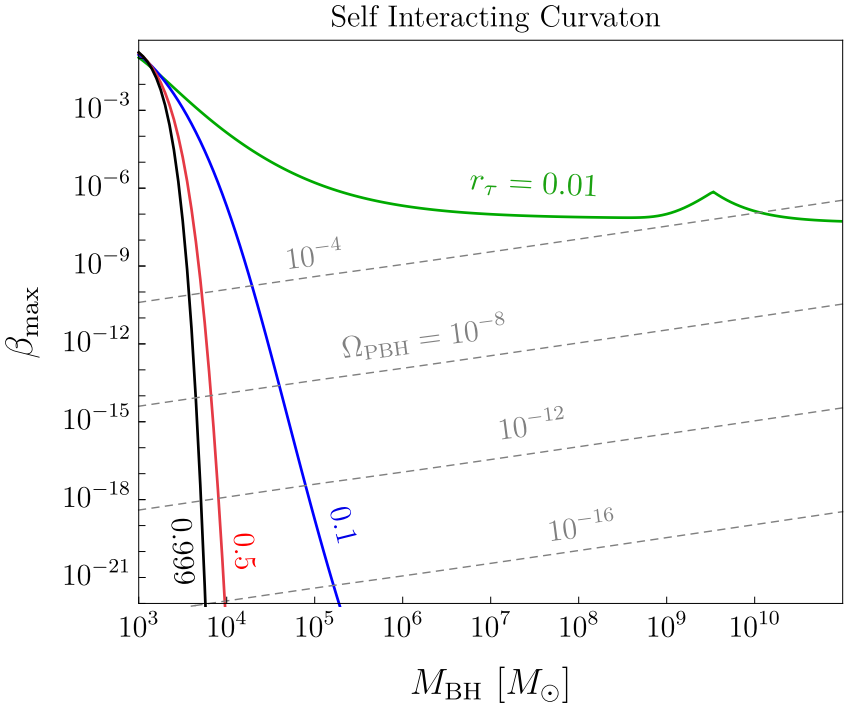

Figure 7. Maximal PBH mass fraction at formation $\beta_{\rm max}$ as a function of PBH mass in the self-interacting curvaton model from Sec. 6.2, where σ_ζ^2 saturates spectral distortion bounds for different values of r_τ, as defined in Eq. (5.11). We take $\zeta_\chi = c_1\,\delta\chi_* + c_2\,\delta\chi_*^2 + c_3\,\delta\chi_*^3$ to take the perturbative form of Eq. (6.14), with sample parameters fixed as $(c_1, c_2, c_3) = (1, 0.5, 0.1)$. For a concrete potential which can realize these values, see Appendix B. Contours of constant $\Omega_{\rm BH}$ today are shown in dashed gray.

where the sum runs over all real roots.

The resulting maximal PBH abundance consistent with spectral distortion constraints is shown in Fig. 7 for a sample set of parameters. Comparison with $\beta_{\rm max}$ in the standard curvaton scenario (see Fig. 6) reveals the dramatic amplification of non-Gaussianity that even weak interactions can afford. Note that while the non-linear growth of modes between horizon exit and the onset of oscillations significantly boosts the potential amount of non-Gaussianity, the curvaton still needs to be very subdominant at the time of its decay ($r_\tau \ll 1$) to yield an appreciable fraction of primordial SMBHs while evading spectral distortion constraints.[17]

7 Conclusions

Much remains to be understood about the origin and evolution of our universe's most massive black holes. The inferred population of supermassive black holes with $M_{\rm BH} \sim 10^6 - 10^{11} M_\odot$ in the high-redshift universe is perhaps surprising, and challenges the standard assumption that these objects formed from low mass seeds which grew through the processes of accretion and mergers. In this study, we have taken this as motivation to consider the possibility that

[17] It is actually even more natural to fulfill this condition here since energy density in the curvaton field dilutes more quickly upon introducing interactions.

some of our universe's supermassive black holes may be primordial in origin, having formed from the direct collapse of overdensities seeded by inflation.

Forming primordial SMBH from direct collapse requires an enhanced power spectrum on small scales ($k \sim 10 - 10^4\,\mathrm{Mpc}^{-1}$), which results in dangerous CMB spectral distortions. Since the CMB exhibits a nearly perfect blackbody spectrum, such distortions exclude the possibility that a population of primordial SMBH could have formed from Gaussian density perturbations. However, if the distribution of primordial curvature perturbations were highly non-Gaussian, it is possible that primordial black holes may have formed from smaller peaks in the power spectrum. To evade limits from spectral distortions, the tail of the probability distribution must be very heavy, falling off as $P_\zeta \sim \exp\left(-|\zeta|^n\right)$ with $n \lesssim 0.6$; we are not aware of any single-field inflationary model that can realize this behavior.

In this paper, we have shown that such heavy-tailed distributions can be generated if a self-interacting curvaton field is also present as a spectator during inflation. In the standard curvaton scenario, non-Gaussianity arises from the inefficient conversion of isocurvature perturbations into adiabatic perturbations when the curvaton decays. However, the degree of non-Gaussianity in this minimal realization is insufficient to yield an appreciable primordial SMBH population. By adding quartic self-interactions, we have found that the non-Gaussian tail can be made significantly heavier, allowing for a viable primordial SMBH population, as shown in Fig. 7.

Finally, this work is especially timely in light of recent pulsar timing array observations. In particular, the NANOGrav collaboration just announced evidence of a signal in its 15-year data set consistent with a stochastic gravitational wave background in the nHz frequency range [117]. The leading astrophysical interpretation of this signal is that it consists of gravitational waves from supermassive black hole binary mergers. However, some aspects of this data, such as the frequency scaling of the spectral density parameter, are not particularly well-fit by this interpretation [118, 119]. Given that the distribution of supermassive black hole binaries would be different if these objects were of a primordial origin, one avenue for future investigation would be to compute the gravitational wave signal predicted in this scenario; see [120] for preliminary work in this direction. There are also other signals, such as scalar-induced secondary gravitational waves, which could offer complimentary evidence of this scenario and deserve further study. Regardless, the recent detection of the gravitational wave background provides us with motivation to better understand the cosmic origin of our universe's supermassive black holes.

Acknowledgments

We would like to thank Wayne Hu and Keisuke Inomata for helpful conversations. AI thanks the organizers and participants of the New Horizons in Primordial Black Hole Physics (NEHOP) workshop, where part of this work was completed. DH, GK and AS are supported by the Fermi Research Alliance, LLC under Contract No. DE-AC02-07CH11359 with the U.S. Department of Energy, Office of Science, Office of High Energy Physics.

References

[1] Y. Shen, G.T. Richards, M.A. Strauss, P.B. Hall, D.P. Schneider, S. Snedden et al., *A catalog of quasar properties from sloan digital sky survey data release 7*, *The Astrophysical Journal Supplement Series* **194** (2011) 45.

[2] E. Bañados, B.P. Venemans, C. Mazzucchelli, E.P. Farina, F. Walter, F. Wang et al., *An 800-million-solar-mass black hole in a significantly neutral Universe at a redshift of 7.5*, *Nature* **553** (2018) 473 [1712.01860].

[3] N.P. Ross and N.J.G. Cross, *The near and mid-infrared photometric properties of known redshift $z \geq 5$ quasars*, *MNRAS* **494** (2020) 789 [1906.06974].

[4] C.J. Willott et al., *The Canada-France High-z Quasar Survey: nine new quasars and the luminosity function at redshift 6*, *Astron. J.* **139** (2010) 906 [0912.0281].

[5] E. Bañados et al., *The Pan-STARRS1 distant $z > 5.6$ quasar survey: more than 100 quasars within the first Gyr of the universe*, *Astrophys. J. Suppl.* **227** (2016) 11 [1608.03279].

[6] L. Jiang, I.D. McGreer, X. Fan, M.A. Strauss, E. Bañados, R.H. Becker et al., *The Final SDSS High-redshift Quasar Sample of 52 Quasars at $z > 5.7$*, *APJ* **833** (2016) 222 [1610.05369].

[7] DES, WISE, VISTA collaboration, *Eight new luminous $z \geq 6$ quasars discovered via SED model fitting of VISTA, WISE and Dark Energy Survey Year 1 observations*, *Mon. Not. Roy. Astron. Soc.* **468** (2017) 4702 [1701.04852].

[8] Y. Matsuoka, K. Iwasawa, M. Onoue, N. Kashikawa, M.A. Strauss, C.-H. Lee et al., *Subaru High-z Exploration of Low-luminosity Quasars (SHELLQs). X. Discovery of 35 Quasars and Luminous Galaxies at $5.7 \leq z \leq 7.0$*, *APJ* **883** (2019) 183 [1908.07910].

[9] J. Yang, F. Wang, X. Fan, X.-B. Wu, F. Bian, E. Bañados et al., *Filling in the Quasar Redshift Gap at $z \sim 5.5$ II: A Complete Survey of Luminous Quasars in the Post-Reionization Universe*, *arXiv e-prints* (2018) arXiv:1810.11927 [1810.11927].

[10] F. Wang, J. Yang, X. Fan, X.-B. Wu, M. Yue, J.-T. Li et al., *Exploring Reionization-era Quasars. III. Discovery of 16 Quasars at $6.4 \lesssim z \lesssim 6.9$ with DESI Legacy Imaging Surveys and the UKIRT Hemisphere Survey and Quasar Luminosity Function at $z \sim 6.7$*, *APJ* **884** (2019) 30 [1810.11926].

[11] B. Mutlu-Pakdil, M.S. Seigar and B.L. Davis, *The local black holes mass function derived from the $m_{BH} - p$ and the $m_{BH} - n$ relations*, *The Astrophysical Journal* **830** (2016) 117.

[12] F. Shankar, D.H. Weinberg and J. Miralda-Escudé, *Accretion-driven evolution of black holes: Eddington ratios, duty cycles and active galaxy fractions*, *Monthly Notices of the Royal Astronomical Society* **428** (2012) 421.

[13] X. Shen, P.F. Hopkins, C.-A. Faucher-Giguère, D.M. Alexander, G.T. Richards, N.P. Ross et al., *The bolometric quasar luminosity function at $z = 0 - 7$*, *Monthly Notices of the Royal Astronomical Society* **495** (2020) 3252.

[14] A. Sicilia, A. Lapi, L. Boco, F. Shankar, D.M. Alexander, V. Allevato et al., *The black hole mass function across cosmic time. II. heavy seeds and (super)massive black holes*, *The Astrophysical Journal* **934** (2022) 66.

[15] N. Banik, J.C. Tan and P. Monaco, *The formation of supermassive black holes from Population III.1 seeds. I. Cosmic formation histories and clustering properties*, *Monthly Notices of the Royal Astronomical Society* **483** (2018) 3592.

[16] E.E. Salpeter, *Accretion of Interstellar Matter by Massive Objects.*, *apj* **140** (1964) 796.

[17] M. Volonteri, *Formation of Supermassive Black Holes*, *Astron. Astrophys. Rev.* **18** (2010) 279 [1003.4404].

[18] Z. Haiman, *Constraints from gravitational recoil on the growth of supermassive black holes at high redshift*, *Astrophys. J.* **613** (2004) 36 [astro-ph/0404196].

[19] S.L. Shapiro, *Spin, accretion and the cosmological growth of supermassive black holes*, *Astrophys. J.* **620** (2005) 59 [astro-ph/0411156].

[20] M. Volonteri and M.J. Rees, *Quasars at z=6: The survival of the fittest*, *Astrophys. J.* **650** (2006) 669 [astro-ph/0607093].

[21] T. Tanaka and Z. Haiman, *The Assembly of Supermassive Black Holes at High Redshifts*, *Astrophys. J.* **696** (2009) 1798 [0807.4702].

[22] SDSS collaboration, *A Survey of $z > 5.8$ quasars in the Sloan Digital Sky Survey I: Discovery of three new quasars and the spatial density of luminous quasars at $z \sim 6$*, *Astron. J.* **122** (2001) 2833 [astro-ph/0108063].

[23] D.J. Mortlock et al., *A luminous quasar at a redshift of $z = 7.085$*, *Nature* **474** (2011) 616 [1106.6088].

[24] X.-B. Wu, F. Wang, X. Fan, W. Yi, W. Zuo, F. Bian et al., *An ultraluminous quasar with a twelve-billion-solar-mass black hole at redshift 6.30*, *Nature* **518** (2015) 512 [1502.07418].

[25] B. Trakhtenbrot, H. Netzer, P. Lira and O. Shemmer, *Black-Hole Mass and Growth Rate at $z \simeq 4.8$: A Short Episode of Fast Growth Followed by Short Duty Cycle Activity*, *Astrophys. J.* **730** (2011) 7 [1012.1871].

[26] H. Netzer, *The Largest black holes and the most luminous galaxies*, *Astrophys. J. Lett.* **583** (2003) L5 [astro-ph/0210548].

[27] P. Natarajan and E. Treister, *Is there an upper limit to black hole masses?*, *Mon. Not. Roy. Astron. Soc.* **393** (2009) 838 [0808.2813].

[28] K. Inayoshi and Z. Haiman, *Is There a Maximum Mass for Black Holes in Galactic Nuclei?*, *APJ* **828** (2016) 110 [1601.02611].

[29] B.J. Carr, *The Primordial black hole mass spectrum*, *Astrophys. J.* **201** (1975) 1.

[30] S.M. Leach, M. Sasaki, D. Wands and A.R. Liddle, *Enhancement of superhorizon scale inflationary curvature perturbations*, *Phys. Rev. D* **64** (2001) 023512 [astro-ph/0101406].

[31] J. Garcia-Bellido and E. Ruiz Morales, *Primordial black holes from single field models of inflation*, *Phys. Dark Univ.* **18** (2017) 47 [1702.03901].

[32] C. Germani and T. Prokopec, *On primordial black holes from an inflection point*, *Phys. Dark Univ.* **18** (2017) 6 [1706.04226].

[33] G. Ballesteros and M. Taoso, *Primordial black hole dark matter from single field inflation*, *Phys. Rev. D* **97** (2018) 023501 [1709.05565].

[34] M.P. Hertzberg and M. Yamada, *Primordial Black Holes from Polynomial Potentials in Single Field Inflation*, *Phys. Rev. D* **97** (2018) 083509 [1712.09750].

[35] S.S. Mishra and V. Sahni, *Primordial black holes from a tiny bump/dip in the inflaton potential*, *JCAP* **2020** (2019) 007 [1911.00057].

[36] K. Inomata, E. McDonough and W. Hu, *Amplification of primordial perturbations from the rise or fall of the inflaton*, *JCAP* **02** (2022) 031 [2110.14641].

[37] Y.-F. Cai, X. Ma, M. Sasaki, D.-G. Wang and Z. Zhou, *Highly non-Gaussian tails and primordial black holes from single-field inflation*, *JCAP* **12** (2022) 034 [2207.11910].

[38] C. Pattison, V. Vennin, H. Assadullahi and D. Wands, *Quantum diffusion during inflation and primordial black holes*, *JCAP* **10** (2017) 046 [1707.00537].

[39] M. Biagetti, G. Franciolini, A. Kehagias and A. Riotto, *Primordial Black Holes from Inflation and Quantum Diffusion*, *JCAP* **07** (2018) 032 [1804.07124].

[40] J.M. Ezquiaga, J. Garcia-Bellido and V. Vennin, *The exponential tail of inflationary fluctuations: consequences for primordial black holes*, *JCAP* **03** (2020) 029 [1912.05399].

[41] C.A. Pattison, V. Vennin, D. Wands and H. Assadullahi, *Ultra-slow-roll inflation with quantum diffusion*, *Journal of Cosmology and Astroparticle Physics* **2021** (2021) .

[42] Y.-F. Cai, X.-H. Ma, M. Sasaki, D.-G. Wang and Z. Zhou, *One small step for an inflaton, one giant leap for inflation: A novel non-Gaussian tail and primordial black holes*, *Phys. Lett. B* **834** (2022) 137461 [2112.13836].

[43] J. Garcia-Bellido, A.D. Linde and D. Wands, *Density perturbations and black hole formation in hybrid inflation*, *Phys. Rev. D* **54** (1996) 6040 [astro-ph/9605094].

[44] S. Clesse and J. Garcia-Bellido, *Massive primordial black holes from hybrid inflation as dark matter and the seeds of galaxies*, *Phys. Rev. D* **92** (2015) 023524.

[45] A.R. Brown, *Hyperbolic Inflation*, *Phys. Rev. Lett.* **121** (2018) 251601 [1705.03023].

[46] G.A. Palma, S. Sypsas and C. Zenteno, *Seeding primordial black holes in multifield inflation*, *Phys. Rev. Lett.* **125** (2020) 121301 [2004.06106].

[47] J. Fumagalli, S. Renaux-Petel, J.W. Ronayne and L.T. Witkowski, *Turning in the landscape: A new mechanism for generating primordial black holes*, *Phys. Lett. B* **841** (2023) 137921 [2004.08369].

[48] M. Braglia, D.K. Hazra, F. Finelli, G.F. Smoot, L. Sriramkumar and A.A. Starobinsky, *Generating PBHs and small-scale GWs in two-field models of inflation*, *JCAP* **08** (2020) 001 [2005.02895].

[49] S. Pi and M. Sasaki, *Primordial Black Hole Formation in Non-Minimal Curvaton Scenario*, 2112.12680.

[50] S.R. Geller, W. Qin, E. McDonough and D.I. Kaiser, *Primordial black holes from multifield inflation with nonminimal couplings*, *Phys. Rev. D* **106** (2022) 063535 [2205.04471].

[51] O. Özsoy and G. Tasinato, *Inflation and Primordial Black Holes*, *Universe* **9** (2023) 203 [2301.03600].

[52] Planck collaboration, *Planck 2018 results. VI. Cosmological parameters*, *Astron. Astrophys.* **641** (2020) A6 [1807.06209].

[53] J.C. Mather et al., *Measurement of the Cosmic Microwave Background spectrum by the COBE FIRAS instrument*, *Astrophys. J.* **420** (1994) 439.

[54] D.J. Fixsen, E.S. Cheng, J.M. Gales, J.C. Mather, R.A. Shafer and E.L. Wright, *The Cosmic Microwave Background spectrum from the full COBE FIRAS data set*, *Astrophys. J.* **473** (1996) 576 [astro-ph/9605054].

[55] Planck collaboration, *Planck 2018 results. IX. Constraints on primordial non-Gaussianity*, *Astron. Astrophys.* **641** (2020) A9 [1905.05697].

[56] Planck collaboration, *Planck 2018 results. X. Constraints on inflation*, *Astron. Astrophys.* **641** (2020) A10 [1807.06211].

[57] J.M. Bardeen, J.R. Bond, N. Kaiser and A.S. Szalay, *The Statistics of Peaks of Gaussian Random Fields*, *Astrophys. J.* **304** (1986) 15.

[58] S. Young and M. Musso, *Application of peaks theory to the abundance of primordial black holes*, *JCAP* **11** (2020) 022 [2001.06469].

[59] C.-M. Yoo, T. Harada, S. Hirano and K. Kohri, *Abundance of Primordial Black Holes in Peak Theory for an Arbitrary Power Spectrum*, *PTEP* **2021** (2021) 013E02 [2008.02425].

[60] W.H. Press and P. Schechter, *Formation of galaxies and clusters of galaxies by selfsimilar gravitational condensation*, *Astrophys. J.* **187** (1974) 425.

[61] M. Shibata and M. Sasaki, *Black hole formation in the Friedmann universe: Formulation and computation in numerical relativity*, *Phys. Rev. D* **60** (1999) 084002 [gr-qc/9905064].

[62] A. Escrivà, C. Germani and R.K. Sheth, *Universal threshold for primordial black hole formation*, *Phys. Rev. D* **101** (2020) 044022 [1907.13311].

[63] V. Atal, J. Cid, A. Escrivà and J. Garriga, *PBH in single field inflation: the effect of shape dispersion and non-Gaussianities*, *JCAP* **05** (2020) 022 [1908.11357].

[64] V. Atal, J. Garriga and A. Marcos-Caballero, *Primordial black hole formation with non-Gaussian curvature perturbations*, *JCAP* **09** (2019) 073 [1905.13202].

[65] C.-M. Yoo, J.-O. Gong and S. Yokoyama, *Abundance of primordial black holes with local non-Gaussianity in peak theory*, *JCAP* **09** (2019) 033 [1906.06790].

[66] A. Kehagias, I. Musco and A. Riotto, *Non-Gaussian Formation of Primordial Black Holes: Effects on the Threshold*, *JCAP* **12** (2019) 029 [1906.07135].

[67] T. Harada, C.-M. Yoo and K. Kohri, *Threshold of primordial black hole formation*, *Phys. Rev. D* **88** (2013) 084051 [1309.4201].

[68] G. Ferrante, G. Franciolini, A. Iovino, Junior. and A. Urbano, *Primordial non-Gaussianity up to all orders: Theoretical aspects and implications for primordial black hole models*, *Phys. Rev. D* **107** (2023) 043520 [2211.01728].

[69] S. Young, C.T. Byrnes and M. Sasaki, *Calculating the mass fraction of primordial black holes*, *JCAP* **07** (2014) 045 [1405.7023].

[70] K. Ando, K. Inomata and M. Kawasaki, *Primordial black holes and uncertainties in the choice of the window function*, *Phys. Rev. D* **97** (2018) 103528 [1802.06393].

[71] R.A. Sunyaev and Y.B. Zeldovich, *Small scale fluctuations of relic radiation*, *Astrophys. Space Sci.* **7** (1970) 3.

[72] Y.B. Zeldovich and R.A. Sunyaev, *The Interaction of Matter and Radiation in a Hot-Model Universe*, *Astrophys. Space Sci.* **4** (1969) 301.

[73] A.F. Illarionov and R.A. Sunyaev, *Why the number of galactic X-ray stars is so small?*, *Astron. Astrophys.* **39** (1975) 185.

[74] W. Hu and J. Silk, *Thermalization and spectral distortions of the cosmic background radiation*, *Phys. Rev. D* **48** (1993) 485.

[75] J. Chluba, A.L. Erickcek and I. Ben-Dayan, *Probing the inflaton: Small-scale power spectrum constraints from measurements of the CMB energy spectrum*, *Astrophys. J.* **758** (2012) 76 [1203.2681].

[76] R. Khatri and R.A. Sunyaev, *Beyond y and μ: the shape of the cmb spectral distortions in the intermediate epoch,* $1.5 \times 10^4 < z < 2 \times 10^5$, *JCAP* **09** (2012) 016 [1207.6654].

[77] J. Chluba and R.A. Sunyaev, *Superposition of blackbodies and the dipole anisotropy: A possibility to calibrate CMB experiments*, *Astronomy & Astrophysics* **424** (2004) 389.

[78] A. Stebbins, *Cmb spectral distortions from the scattering of temperature anisotropies*, 2007. 10.48550/ARXIV.ASTRO-PH/0703541.

[79] J. Chluba and R.A. Sunyaev, *The evolution of CMB spectral distortions in the early Universe*, *Mon. Not. Roy. Astron. Soc.* **419** (2012) 1294 [1109.6552].

[80] C. Pitrou and A. Stebbins, *Parameterization of temperature and spectral distortions in future CMB experiments*, *General Relativity and Gravitation* **46** (2014) .

[81] B.J. Carr and J.E. Lidsey, *Primordial black holes and generalized constraints on chaotic inflation*, *Physical Review D* **48** (1993) 543.

[82] J. Chluba, *Which spectral distortions does ΛCDM actually predict?*, *Mon. Not. Roy. Astron. Soc.* **460** (2016) 227 [1603.02496].

[83] A.M. Green and B.J. Kavanagh, *Primordial Black Holes as a dark matter candidate*, *J. Phys. G* **48** (2021) 043001 [2007.10722].

[84] S. Bird, H.V. Peiris, M. Viel and L. Verde, *Minimally Parametric Power Spectrum Reconstruction from the Lyman-alpha Forest*, *Mon. Not. Roy. Astron. Soc.* **413** (2011) 1717 [1010.1519].

[85] C.T. Byrnes, P.S. Cole and S.P. Patil, *Steepest growth of the power spectrum and primordial black holes*, *JCAP* **06** (2019) 028 [1811.11158].

[86] S. Ando, N. Hiroshima and K. Ishiwata, *Constraining the primordial curvature perturbation using dark matter substructure*, *Phys. Rev. D* **106** (2022) 103014 [2207.05747].

[87] T. Nakama, T. Suyama and J. Yokoyama, *Supermassive black holes formed by direct collapse of inflationary perturbations*, *Phys. Rev. D* **94** (2016) 103522 [1609.02245].

[88] M.H. Namjoo, H. Firouzjahi and M. Sasaki, *Violation of non-Gaussianity consistency relation in a single field inflationary model*, *EPL* **101** (2013) 39001 [1210.3692].

[89] X. Chen, H. Firouzjahi, M.H. Namjoo and M. Sasaki, *A Single Field Inflation Model with Large Local Non-Gaussianity*, *EPL* **102** (2013) 59001 [1301.5699].

[90] X. Chen, H. Firouzjahi, E. Komatsu, M.H. Namjoo and M. Sasaki, *In-in and δN calculations of the bispectrum from non-attractor single-field inflation*, *JCAP* **12** (2013) 039 [1308.5341].

[91] Y.-F. Cai, X. Chen, M.H. Namjoo, M. Sasaki, D.-G. Wang and Z. Wang, *Revisiting non-Gaussianity from non-attractor inflation models*, *JCAP* **05** (2018) 012 [1712.09998].

[92] D.S. Salopek and J.R. Bond, *Nonlinear evolution of long wavelength metric fluctuations in inflationary models*, *Phys. Rev. D* **42** (1990) 3936.

[93] A.A. Starobinsky, *Dynamics of Phase Transition in the New Inflationary Universe Scenario and Generation of Perturbations*, *Phys. Lett. B* **117** (1982) 175.

[94] M. Sasaki and E.D. Stewart, *A General analytic formula for the spectral index of the density perturbations produced during inflation*, *Prog. Theor. Phys.* **95** (1996) 71 [astro-ph/9507001].

[95] M. Sasaki and T. Tanaka, *Superhorizon scale dynamics of multiscalar inflation*, *Prog. Theor. Phys.* **99** (1998) 763 [gr-qc/9801017].

[96] D.H. Lyth, K.A. Malik and M. Sasaki, *A General proof of the conservation of the curvature perturbation*, *JCAP* **05** (2005) 004 [astro-ph/0411220].

[97] D.H. Lyth and Y. Rodriguez, *The Inflationary prediction for primordial non-Gaussianity*, *Phys. Rev. Lett.* **95** (2005) 121302 [astro-ph/0504045].

[98] A.A. Starobinsky, *Stochastic de Sitter (Inflationary) Stage in the Early Universe*, *Lect. Notes Phys.* **246** (1986) 107.

[99] V. Vennin and A.A. Starobinsky, *Correlation Functions in Stochastic Inflation*, *Eur. Phys. J. C* **75** (2015) 413 [1506.04732].

[100] Y. Tada and V. Vennin, *Statistics of coarse-grained cosmological fields in stochastic inflation*, *JCAP* **02** (2022) 021 [2111.15280].

[101] H. Firouzjahi, A. Nassiri-Rad and M. Noorbala, *Stochastic Ultra Slow Roll Inflation*, *JCAP* **01** (2019) 040 [1811.02175].

[102] V. Atal, A. Sanglas and N. Triantafyllou, *NANOGrav signal as mergers of Stupendously Large Primordial Black Holes*, *JCAP* **06** (2021) 022 [2012.14721].

[103] D.H. Lyth and D. Wands, *Generating the curvature perturbation without an inflaton*, *Phys. Lett. B* **524** (2002) 5 [hep-ph/0110002].

[104] T. Moroi and T. Takahashi, *Effects of cosmological moduli fields on cosmic microwave background*, *Phys. Lett. B* **522** (2001) 215 [hep-ph/0110096].

[105] N. Bartolo and A.R. Liddle, *The Simplest curvaton model*, *Phys. Rev. D* **65** (2002) 121301 [astro-ph/0203076].

[106] S. Mollerach, *Isocurvature Baryon Perturbations and Inflation*, *Phys. Rev. D* **42** (1990) 313.

[107] M. Sasaki, J. Valiviita and D. Wands, *Non-Gaussianity of the primordial perturbation in the curvaton model*, *Phys. Rev. D* **74** (2006) 103003 [astro-ph/0607627].

[108] D. Langlois, F. Vernizzi and D. Wands, *Non-linear isocurvature perturbations and non-Gaussianities*, *JCAP* **12** (2008) 004 [0809.4646].

[109] N. Bartolo, S. Matarrese and A. Riotto, *On nonGaussianity in the curvaton scenario*, *Phys. Rev. D* **69** (2004) 043503 [hep-ph/0309033].

[110] K. Enqvist, S. Nurmi, O. Taanila and T. Takahashi, *Non-Gaussian Fingerprints of Self-Interacting Curvaton*, *JCAP* **04** (2010) 009 [0912.4657].

[111] K. Enqvist, S. Nurmi, G. Rigopoulos, O. Taanila and T. Takahashi, *The Subdominant Curvaton*, *JCAP* **11** (2009) 003 [0906.3126].

[112] O. Taanila, *Primordial Perturbations from a Self-interacting Curvaton*, Ph.D. thesis, Helsinki U., 2010.

[113] K. Enqvist, *The self-interacting curvaton*, *Prog. Theor. Phys. Suppl.* **190** (2011) 62 [1012.1711].

[114] J. Fonseca and D. Wands, *Non-Gaussianity and Gravitational Waves from Quadratic and Self-interacting Curvaton*, *Phys. Rev. D* **83** (2011) 064025 [1101.1254].

[115] G. Domènech and M. Sasaki, *Conformal Frame Dependence of Inflation*, *JCAP* **04** (2015) 022 [1501.07699].

[116] K. Enqvist, S. Nurmi, G. Rigopoulos, O. Taanila and T. Takahashi, *The Subdominant Curvaton*, *JCAP* **11** (2009) 003 [0906.3126].

[117] NANOGrav collaboration, *The NANOGrav 15 yr Data Set: Evidence for a Gravitational-wave Background*, *Astrophys. J. Lett.* **951** (2023) L8 [2306.16213].

[118] NANOGrav collaboration, *The NANOGrav 15-year Data Set: Bayesian Limits on Gravitational Waves from Individual Supermassive Black Hole Binaries*, 2306.16222.

[119] NANOGrav collaboration, *The NANOGrav 15-year Data Set: Constraints on Supermassive Black Hole Binaries from the Gravitational Wave Background*, 2306.16220.

[120] Y. Gouttenoire, S. Trifinopoulos, G. Valogiannis and M. Vanvlasselaer, *Scrutinizing the Primordial Black Holes Interpretation of PTA Gravitational Waves and JWST Early Galaxies*, 2307.01457.

[121] J.M. Bardeen, *Gauge Invariant Cosmological Perturbations*, *Phys. Rev. D* **22** (1980) 1882.

A The δN Formalism

A.1 Review

The δN formalism [92–97, 108] is a technique for computing the non-linear curvature perturbation ζ on large scales by identifying it with the perturbed logarithmic expansion from some initial state to a final state of fixed energy density. In a homogenous background, the number of e-folds elapsed between two moments of times t_1 and t_2 is

$$\bar{N}(t_2, t_1) = \int_{t_1}^{t_2} dt\, H\,. \tag{A.1}$$

Meanwhile, the amount of expansion in a perturbed universe is [96]

$$N(t_2, t_1; \vec{x}) = \int_{t_1}^{t_2} dt\, (H + \dot{\psi})\,, \tag{A.2}$$

where ψ is the curvature perturbation appearing in the decomposition of the spatial 3-metric $g_{ij} = a^2(t)e^{2\psi(t,\vec{x})}\delta_{ij}$.[18] Note that this expression holds on superhorizon scales, where spatial gradients can be neglected. We define $\delta N \equiv N(t_2, t_1; x) - \bar{N}(t_2, t_1)$ to be the difference between the perturbed and unperturbed expansion, and see that it equates to the change in the curvature perturbation from an initial hypersurface at t_1 to a final hypersurface at t_2

$$\delta N \equiv N(t_2, t_1; \vec{x}) - \bar{N}(t_2, t_1) = \psi(t_2, \vec{x}) - \psi(t_1, \vec{x})\,. \tag{A.3}$$

Equivalently, the change in ψ going from one choice of slicing to another is the difference between the actual number of e-folds N and the homogenous background value $\bar{N}$.

Since the curvature perturbation ψ is a gauge-dependent quantity, whose value depends on the choice of slicing, it is convenient to combine this with the gauge-dependent density perturbation $\delta\rho$ to form the gauge-invariant curvature perturbation [121]:

$$\zeta(t, \vec{x}) = \psi(t, \vec{x}) + \frac{1}{3}\int_{\bar{\rho}(t)}^{\rho(t,\vec{x})} \frac{d\rho}{(1+w)\rho}\,, \tag{A.4}$$

where w is the equation of state of the cosmological fluid, $\rho(t, \vec{x})$ is the inhomogenous local energy density, and $\bar{\rho}(t)$ is the homogenous background energy density. It was demonstrated in Ref. [96] that this quantity is conserved on superhorizon scales.

We would like to equate this gauge-invariant, conserved curvature perturbation ζ with the perturbed logarithmic expansion δN. By choosing the initial hypersurface at t_1 to be spatially flat, such that $\psi(t_1, \vec{x}) = 0$, from Eq. (A.3) we can equate $\delta N(t_2, t_1; \vec{x} = \psi(t_2, \vec{x})$. By choosing the finial hypersurface at t_2 to be uniform density, such that $\rho(t_2, \vec{x}) = \bar{\rho}(t_2)$, from Eq. (A.4) we have $\zeta(t_2, \vec{x}) = \psi(t_2, \vec{x})$. Combining these expressions gives the δN formula

$$\zeta(t_2, \vec{x}) = \delta N(t_2, t_1; \vec{x})\,, \tag{A.5}$$

relating the curvature perturbation with the perturbed expansion between a spatially flat and uniform energy density hypersurface.

A.2 Numerical Implementation

It is also possible to implement the δN formalism numerically. Following inflaton decay, the exact system of equations describing the evolution of the curvaton and radiation bath is

$$\ddot{\chi} + \left(3H + \frac{1}{\tau}\right)\dot{\chi} + V'_\chi = 0 \quad , \quad \dot{\rho}_R + 4H\rho_R = \frac{\dot{\chi}^2}{\tau} \quad , \quad H^2 = \frac{8\pi}{3M_{\rm Pl}^2}(\rho_R + \rho_\chi)\,. \tag{A.6}$$

We set the initial conditions at the end of inflation by specifying $\chi_i = \chi_*$, $\dot{\chi}_i = 0$, and $H_i = H_*$, which in turn determines $\rho_{R,i} = \frac{3M_{\rm Pl}^2}{8\pi}H_i^2 - V_\chi(\chi_i)$. The system of equations should be evolved until a final time t_f satisfying $H_f \ll \tau^{-1}$, such that the curvaton has decayed completely. The number of e-folds elapsed is then computed as $N = \ln(a_f/a_i)$. This procedure should then be repeated for the perturbed field value $\chi_* + \delta\chi_*$, with the fluctuation determined by the size of Hubble at horizon exit $\delta\chi_* = H_*/2\pi$. Evolving until the same final hypersurface of fixed energy density, the curvature perturbation is computed as:

$$\zeta = N(\chi_* + \delta\chi_*) - N(\chi_*)\,. \tag{A.7}$$

Repeating for many different $\delta\chi_*$ gives a functional relation between ζ and the Gaussian $\delta\chi_*$. We leave an in-depth numerical study to future investigation.

[18] We ignore tensor perturbations.

B Weak Quartic Interactions

The sample parameters of Fig. 7 can be obtained rather generically for a variety of weakly interacting models. For concreteness, consider the quartic potential:

$$V_\chi = \frac{1}{2} m_\chi^2 \chi^2 + \frac{\lambda}{4} \chi^4 \,. \tag{B.1}$$

In the limit of small interactions, we can find an explicit functional form for the amplitude at the onset of quadratic oscillations $\chi_0(\chi_*)$ by treating the quartic term as a perturbation. We expand the solution as:

$$\chi_0 = \chi_0^{(0)} + \lambda \chi_0^{(1)} \,. \tag{B.2}$$

At zeroth order in λ, the equation for $\chi_0^{(0)}$ reads:

$$\ddot{\chi}_0^{(0)} + \frac{3}{2t} \dot{\chi}_0^{(0)} + m_\chi^2 \chi_0^{(0)} = 0 \,, \tag{B.3}$$

where we have assumed radiation domination such that $H = 1/2t$. The general solution is

$$\chi_0^{(0)} = A_0 \, w_{1/4}(m_\chi t) + B_0 \, w_{-1/4}(m_\chi t) \,, \tag{B.4}$$

where $w_{1/4}(m_\chi t) \equiv J_{1/4}(m_\chi t)/(m_\chi t)^{1/4}$ and $w_{-1/4}(m_\chi t) \equiv J_{-1/4}(m_\chi t)/(m_\chi t)^{1/4}$, with J Bessel functions of the first kind. For convenience we take evolution to start at $t_{\rm int} = 0$; demanding regularity here instructs us to set $B_0 = 0$. The initial condition $\chi_0|_{t=0} = \chi_*$ fixes $A_0 = 2^{1/4}\,\Gamma(5/4)\,\chi_* \simeq 1.078\,\chi_*$, such that:

$$\chi_0^{(0)} = 1.078\,\chi_* \, \frac{J_{1/4}(m_\chi t)}{(m_\chi t)^{1/4}} \,. \tag{B.5}$$

At first order in λ, the correction satisfies

$$\ddot{\chi}_0^{(1)} + \frac{3}{2t} \dot{\chi}_0^{(1)} + m_\chi^2 \chi_0^{(1)} = - \left(\chi_0^{(0)} \right)^3 \,. \tag{B.6}$$

This second order non-linear differential equation can be solved with the method of variation of parameters, wherein we take the Ansatz:

$$\chi_0^{(1)} = A_1(t) \, w_{1/4}(m_\chi t) + B_1(t) \, w_{-1/4}(m_\chi t) \,. \tag{B.7}$$

The corresponding system of equations for $\dot{A}_1$ and $\dot{B}_1$ is

$$\begin{aligned} &\dot{A}_1 \, w_{1/4}(m_\chi t) + \dot{B}_1 \, w_{-1/4}(m_\chi t) = 0 \\ &\dot{A}_1 \, \dot{w}_{1/4}(m_\chi t) + \dot{B}_1 \, \dot{w}_{-1/4}(m_\chi t) = - \left(\chi_0^{(0)} \right)^3 \,, \end{aligned} \tag{B.8}$$

with integral solutions

$$\begin{aligned} A_1 &= A_0^3 \int dt \, \frac{w_{-1/4}(m_\chi t)\, w_{1/4}(m_\chi t)^3}{w_{1/4}(m_\chi t)\, \dot{w}_{-1/4}(m_\chi t) - \dot{w}_{1/4}(m_\chi t)\, w_{-1/4}(m_\chi t)} \,, \\ B_1 &= -A_0^3 \int dt \, \frac{w_{1/4}(m_\chi t)^4}{w_{1/4}(m_\chi t)\, \dot{w}_{-1/4}(m_\chi t) - \dot{w}_{1/4}(m_\chi t)\, w_{-1/4}(m_\chi t)} \,. \end{aligned} \tag{B.9}$$

We should integrate these from the onset of interactions $t_{\rm int} = 0$ to the onset of oscillations, corresponding to $m_\chi t \sim 1$, with the result:

$$A_1 \simeq -0.689 \frac{\chi_*^3}{m_\chi^2}\,, \quad B_1 \simeq 0.535 \frac{\chi_*^3}{m_\chi^2}\,. \tag{B.10}$$

The full solution is then

$$\chi_0 \simeq 1.078\,\chi_* \frac{J_{1/4}(m_\chi t)}{(m_\chi t)^{1/4}} + \lambda \left(-0.689\,\frac{J_{1/4}(m_\chi t)}{(m_\chi t)^{1/4}} + 0.535\,\frac{J_{-1/4}(m_\chi t)}{(m_\chi t)^{1/4}} \right) \frac{\chi_*^3}{m_\chi^2}\,. \tag{B.11}$$

Finally evaluating this at $m_\chi t \sim 1$ gives

$$\chi_0 \simeq 0.81\,\chi_* - 0.16\,\lambda \frac{\chi_*^3}{m_\chi^2}\,. \tag{B.12}$$

This expression can then be substituted into Eq. (6.14) to obtain ζ_χ. We see for example that the benchmark point of Fig. 7 can be realized for $(\chi_*,\, m_\chi,\, \lambda) = (3.6,\, 1,\, 0.5)$.